Carrier transport in mesoscopic silicon-coupled superconducting junctions

W. M. van Huffelen, T. M. Klapwijk, D. R. Heslinga, M. J. de Boer, and N. van der Post
Department of Applied Physics and Materials Science Centre, University of Groningen, Nijenborgh 4, 9747 AG Groningen, The Netherlands

(Received 12 June 1992; revised manuscript received 29 October 1992)

An overview is presented of experimental results on supercurrent flow and transport at finite voltages in a well-characterized, sandwich-type superconductor-semiconductor-superconductor junction. Carrier transport through the structure is found to be dominated by the interfaces. At low temperatures, inelastic scattering is negligible in the intermediate silicon layer and the system is mesoscopic. Application of a voltage results in a strongly nonthermal carrier distribution in the bulk of the semiconductor. The details of the distribution depend on elastic and Andreev scattering at the interfaces and are directly reflected by the measured current-voltage characteristics. The supercurrent is well described by a recent theory for the proximity effect that takes into account the reduction of the superconducting order parameter across the superconductor-semiconductor interface. Supercurrent measurements to identify a possible interplay between the superconductor phase and the single carrier phase in the semiconductor are discussed.

I. INTRODUCTION

Josephson supercurrent flow is a phenomenon studied in a large variety of superconducting weak-link structures. The usual Josephson junction consists of a thin insulating barrier sandwiched between two superconductors. A well-known alternative is a superconductor– normal-metal–superconductor (SNS) junction, proposed theoretically by DeGennes[1] and subsequently studied experimentally by Clarke.[2] In the original theoretical description the supercurrent flow is understood in terms of the proximity effect. Superconducting Cooper pairs diffuse from the superconductor into the normal metal over a characteristic length which depends on carrier concentration and elastic scattering. If the normal metal is thin compared to the decay length, a supercurrent will flow.[3] Very recently, interest has revived in several older theoretical ideas[4,5] in which ballistic transport through the normal metal N is assumed.[6–9] In this case, phase coherence in N governs electronic transport and the supercurrent is believed to be carried by the discrete excitation spectrum in the normal metal.

A special category of SNS junctions is realized by replacing the normal metal by a degenerately doped semiconductor Sm. In the SSmS system, the coupling strength between the superconductors can be changed by varying the carrier concentration in S, resulting in a variable supercurrent. In principle, transport through Sm could be ballistic, but such a system has not yet been realized. A promising candidate is a high-mobility two-dimensional electron gas (2DEG). Recently it was predicted that a short and narrow ballistic constriction in a 2DEG, carrying a supercurrent I_c, should exhibit a stepwise increase of I_c with the width of the contact.[8,10]

The promise of supercurrent control through variation of the carrier concentration has resulted in much interest for the application of SSmS junctions as ultrafast, low-power, electronic devices. During the last two decades several semiconductor coupled weak links based on various materials and geometries have been reported[11] that carry large supercurrents. The operation of a superconducting field-effect transistor, with a gate electrode controlling the carrier concentration and thereby the supercurrent, has recently been demonstrated.[12–14] Despite the successful fabrication, the electrical behavior of SSmS structures has not been understood.

In this paper we present an overview of experimental results on supercurrent flow and transport at finite voltages in a model system consisting of a thin silicon membrane sandwiched between two superconducting electrodes. The system is well characterized and provides a well-defined current path, allowing for a thorough comparison of the measurements to several existing theories on carrier transport in dirty SSmS systems. It is shown that the SSmS junction cannot be described as a simple SNS system, with the degenerately doped semiconductor acting as a low carrier density normal metal. Instead, the behavior is dominated by the superconductor-semiconductor interfaces. As will be shown, inelastic scattering is negligible and the semiconductor is in the mesoscopic regime. Application of a voltage results in a strongly nonthermal carrier distribution in the bulk of the semiconductor. The details of the distribution depend on elastic and Andreev scattering at the interfaces and are directly reflected by the measured current-voltage (I,V) characteristics. We find that the supercurrent is best described in terms of the recent theory of Kupriyanov and Lukichev[15] that takes into account the reduction of the superconducting order parameter across the S-Sm interface. Because the semiconductor is mesoscopic, an interplay between the phases of the superconductors and the single electron phase in Sm could occur. We discuss supercurrent measurements to identify effects of this nature.

The organization of this paper is as follows. After a general introduction on the fabrication of membrane cou-

pled weak links and overall results, measurements of the voltage carrying state of the junction are discussed. Next, the behavior of the supercurrent as a function of temperature, magnetic field, and rf-radiation is treated and the paper ends with a summary and conclusions.

II. DEVICE FABRICATION AND GENERAL RESULTS

The experimental system studied is shown in Fig. 1. It consists of a very thin, single-crystalline silicon membrane sandwiched between two niobium electrodes. The membrane is obtained[16] by locally etching through a silicon wafer with a degenerately boron-doped surface layer (doping level about 7×10^{19} cm^{-3}). A shallow implantation is used to ensure that the thickness of the doped layer is about 50 nm. A wet anisotropic etch is applied to the opposite side. It stops at the doped layer resulting in a thin slice of heavily doped silicon, which is uniform to within 10 nm over the entire surface of 900 μm^2. Scanning electron microscope pictures of broken membrane edges (Fig. 2) yield the thickness L which lies between 40 and 60 nm for different membranes we have studied. Since the method is destructive, the thickness of samples discussed below has not been measured and the average value $L=50$ nm is used. The current-carrying area of the junction is varied by opening a contact window in the insulating silicon nitride (Si_3N_4) layer on top of the membrane, using standard photolithography. After opening the window, the silicon surface is thoroughly cleaned using standard chemical methods. Subsequently the sample is brought into a UHV chamber and covered on both sides with 300-nm electron-beam-evaporated niobium. The main experimental results reported here do not depend on the junction area, which has been varied from 2 to 600 μm^2.

The majority of semiconductor coupled weak links realized to date have either a coplanar or a ridge-type geometry.[11] In these geometries the current path is not well known. The voltage drop along the S-Sm interfaces is position dependent and the current at finite voltages takes a different path than the supercurrent. These complications are not encountered in the present system. The sandwich geometry of this structure ensures a well-defined junction area as well as a known path length of the supercurrent in the semiconductor.

In Fig. 3(a) a typical current-voltage (I,V) characteristic for a 35-μm^2 sample, measured at a temperature of 1.2 K, is displayed. A number of samples of various sizes have been studied, all showing the same general features. The inset shows the presence of a supercurrent up to I_c at $V=0$. For high voltages, above 3–4 mV, a linear slope is found which intercepts the vertical axis at negative current values. This phenomenon has been reported previously in coplanar devices with silicon[17] and $In_xGa_{1-x}As$ (Ref. 18) and in step-edge junctions with a

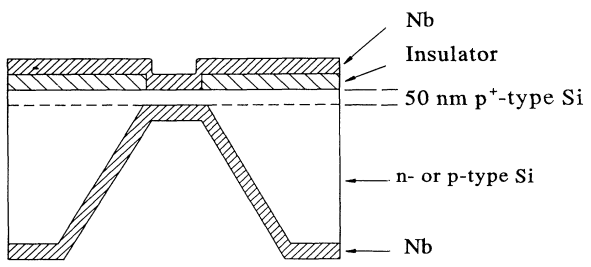

FIG. 1. Niobium-silicon-niobium junction based on a single-crystal silicon membrane.

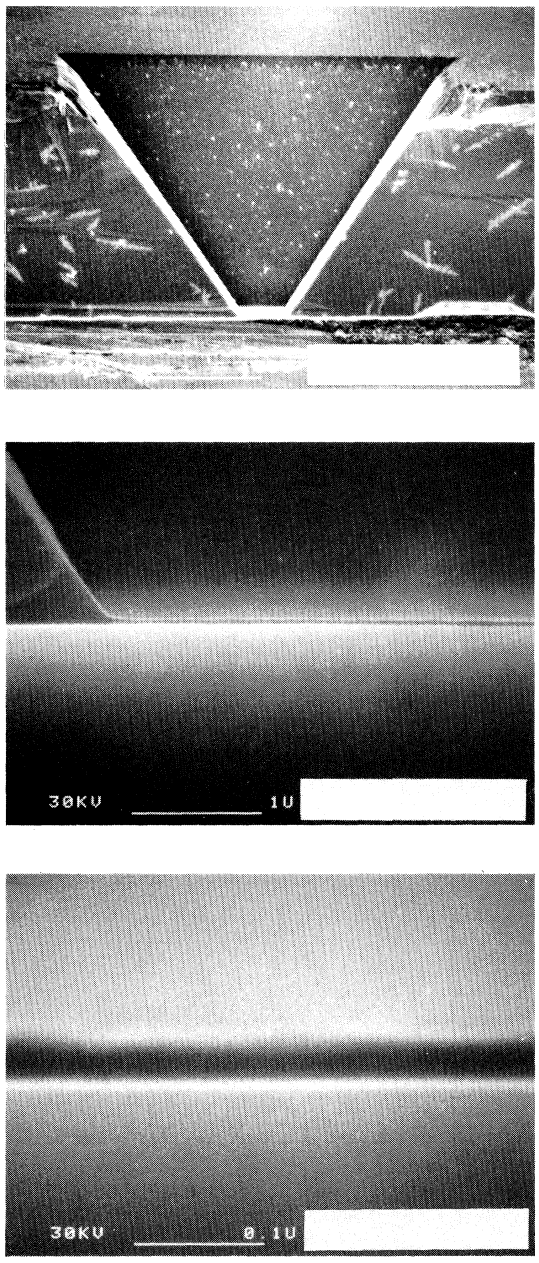

FIG. 2. Scanning electron microscope photographs of a silicon membrane cross section. (a) Full cross-section of the part of the chip containing the etchpit. The width of the pyramidal pit at the top surface is about 400 μm, the width of the membrane at the bottom of the pit equals 40 μm. (b) Corner of the bottom of the pit plus membrane. (c) Detail of the membrane.

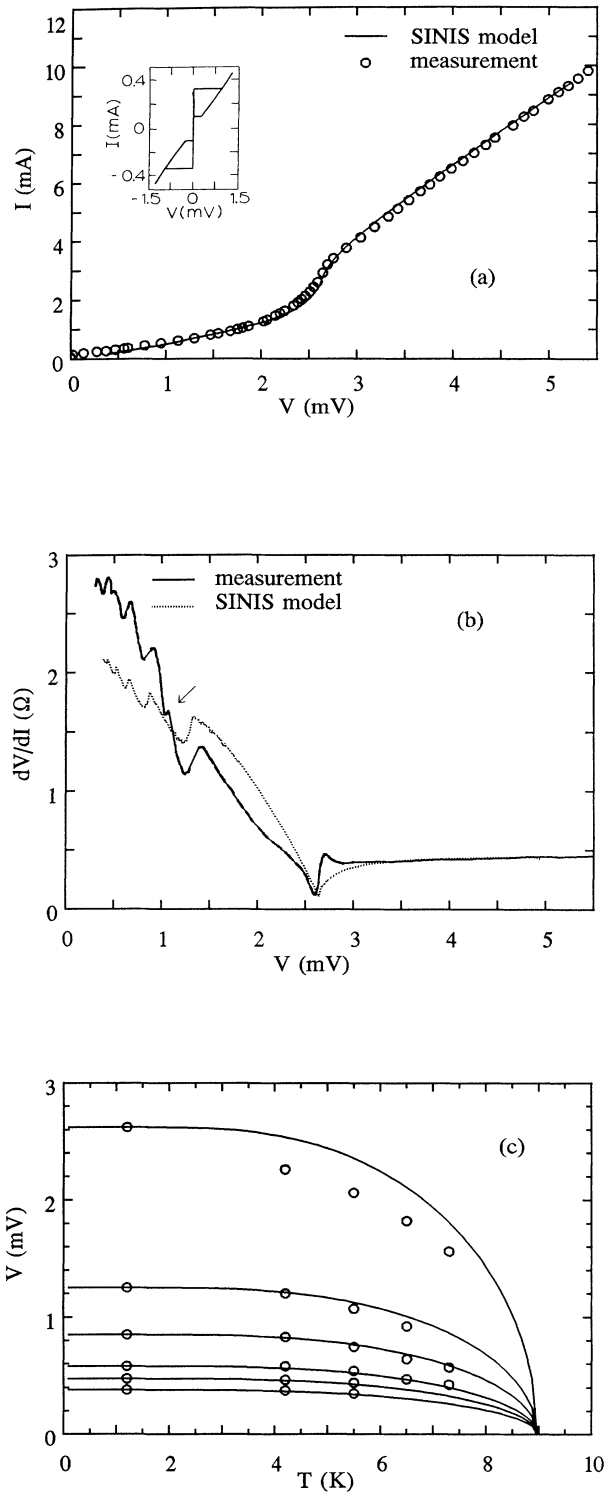

FIG. 3. (a) Current and (b) differential resistance vs voltage for a 35-μm^2 sample, at 1.2 K. The inset in (a) shows the supercurrent. Theoretical curves are calculated from the OBTK model with $Z_1 = Z_2 = 2.0$. The origin of the structure marked with an arrow is unknown. It is absent in other samples. The temperature dependence of the subharmonic gap structure at $eV \approx 2\Delta/n$ is shown in (c) (dots), and compared to the familiar BCS temperature dependence of the gap (solid lines).

Nb/Si interlayer,[19] and is generally called a "current deficit." In addition, a clear signature of the superconducting energy gap of niobium at voltages of 2.9 mV or lower is found. This can be seen more clearly in the measurement of the differential resistance dV/dI as a function of voltage [Fig. 3(b)]. A sharp dip is observed at twice the superconducting energy gap of niobium Δ_{Nb}, together with minima at voltages roughly equal to $2\Delta_{Nb}/ne$, with $n = 2,3,4,5,6$. This structure has been extensively studied in microbridges and is generally called a subharmonic energy gap structure (SGS). The highest order that is observed varies from sample to sample, n ranging from at least 2 to at most 7. The temperature dependence of the position of the dips for the 35-μm^2 sample has been displayed in Fig. 3(c) (dots). For increasing temperature, the measured position of the higher n dips follows the BCS temperature dependence of the gap closely. The deviation of the position of the $n = 1$ dips is believed to be caused by heating of the sample and will be discussed in Sec. III C.

In a separate experiment we have measured the bulk resistivity ρ of the silicon membrane using a standard four-point probe array on top of the membrane. The array is obtained by etching four micron-sized holes in the insulating layer, instead of the large contact window shown in Fig. 1. We find $\rho = (7.7 \pm 1.0) \times 10^{-4}$ Ω cm at 4.2 K and $\rho = (10.0 \pm 1.5) \times 10^{-4}$ Ω cm at 300 K. Using standard free-electron parameters and the expression $\mu = 1/ne\rho$ for the drift-mobility μ (n is the carrier concentration), a mean free path l for elastic scattering of about 5 nm is obtained ($T = 4.2$ K), indicating that the carriers undergo some elastic scattering in the bulk of the silicon. Inelastic-scattering lengths for degenerately doped n-Si have been found from magnetoconductance measurements to be 0.4 μm at 1.2 K and 0.1 μm at 4.2 K.[20] Using these values as a guideline, we expect inelastic scattering to be unimportant in the Si membrane at the lowest temperatures. As we will show, this is consistent with the presence of subharmonic gap structure in the I, V characteristics.

III. VOLTAGE CARRYING STATE

A. The OTBK model

The explanation for subharmonic gap structure was originally given by Klapwijk, Blonder, and Tinkham[21] while the presence of this structure together with a current-deficit is implied in a theoretical model subsequently presented by Octavio *et al.* (OTBK).[22,23] In this section their results are extended to take into account the presence of two nonidentical NS interfaces. The model describes a SNS structure with elastic scattering lumped at the NS interfaces, represented by a δ-function potential of variable height $V(x) = H\delta(x)$. At the interfaces three processes occur: transmission, elastic scattering, and Andreev scattering.[24] The probabilities for these processes are represented by $T(E)$, $B(E)$ and $A(E)$, respectively.[25] They depend on the strength of the interface barrier which is represented by the dimensionless pa-

rameter $Z=H/\hbar v_F$. Z has a simple interpretation: in the normal state the transmission coefficient of the interface barrier is $(1+Z^2)^{-1}$. For simplicity, nonequilibrium phenomena are assumed to be absent in the superconducting electrodes. In this so-called SINIS structure (Fig. 4), where I represents the barrier at the interface, it is further assumed that inelastic scattering is absent in the normal region N between the two interfaces. This implies that energy distribution functions of carriers in N are position independent and reflect only the acceleration due to the applied voltage V. Although in this model the voltage drop will appear completely across the interface barriers, the energy gain eV upon traversal of the structure does not depend on the actual spatial distribution of the potential.

With these assumptions the quasiparticles in N can be separated into two subpopulations, depending on their direction of motion, $f_{\rightarrow}(E,x)$ and $f_{\leftarrow}(E,x)$, which differ from the equilibrium Fermi function $f_0(E)$. In Ref. 22, expressions are derived for $f_{\rightarrow}(E,x)$ and $f_{\leftarrow}(E,x)$ for the case of two identical NS interfaces. Distinguishing the left and right interfaces by subscripts 1 and 2, respectively, we obtain [using Eqs. (1) and (2) of Ref. 22] the following equation for nonidentical interfaces:

$$
\begin{aligned}
&[1-B_1(E)B_2(E+eV)]f_{\rightarrow}(E)-A_1(E)A_2(-E+eV)f_{\rightarrow}(E-2eV)\\
&\quad+A_1(E)B_2(-E+eV)f_{\rightarrow}(-E)+B_1(E)A_2(E+eV)f_{\rightarrow}(-E-2eV)\\
&\qquad=A_1(E)-A_1(E)A_2(-E+eV)+B_1(E)A_2(E+eV)+T_1(E)f_0(E)+B_1(E)T_2(E+eV)f_0(E+eV)\\
&\qquad\quad-A_1(E)T_2(-E+eV)f_0(-E+eV)\ . \qquad (1)
\end{aligned}
$$

This equation expresses $f_{\rightarrow}(E)$ in terms of the same function with its argument shifted by ± 2 eV, and products of the known functions $A(E)$, $B(E)$, $T(E)$, and $f_0(E)$. In principle, it represents an infinite set of recurrent equations. However, the set can be cutoff because $f_{\rightarrow}(E)$ will approach 0 for very high energy and 1 for very low energy. Solving the set self-consistently, $f_{\rightarrow}(E)$ is obtained. Once this function is found, $f_{\leftarrow}(E)$ is easily calculated from it.[22] The current can be found by integrating over the distributions

$$I=2N(0)ev_F A\int dE\,[f_{\rightarrow}(E)-f_{\leftarrow}(E)] \qquad (2)$$

with $N(0)$ the normal-metal single spin density of states at the Fermi level, v_F the Fermi velocity, and A the current-carrying area. Introducing $R_0=1/[2N(0)e^2v_F A]$, the prefactor in Eq. (2) can be written as $1/eR_0$. We note that in our previous Rapid Communication,[26] as well as in a paper by Flensberg, Bindslev Hansen, and Octavio,[27] the prefactor has erroneously been written as $1/eR_N$. The normal-state resistance R_N is determined by the transition of the interfaces, as is shown below in Eq. (5). The outcome of the calculations presented in Refs. 26 and 27 is correct.

In Fig. 5 we have plotted $[f_{\rightarrow}(E)-f_{\leftarrow}(E)]$ in the normal region (high values are black), which is a measure for the current flowing at energy level E, for a SINIS structure with $Z_1=Z_2=2$. The voltage across the junction equals $4\Delta/e$. The energy scale is plotted vertically, whereas the density of states in the superconducting electrodes is plotted horizontally (filled states have been shaded). Most of the current flows at energy levels in N lying between the two superconducting energy gaps. Levels

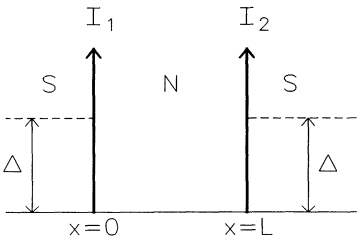

FIG. 4. SINIS structure: SNS structure with nonidentical barriers I_1 and I_2 at the NS interfaces at $x=0$ and L.

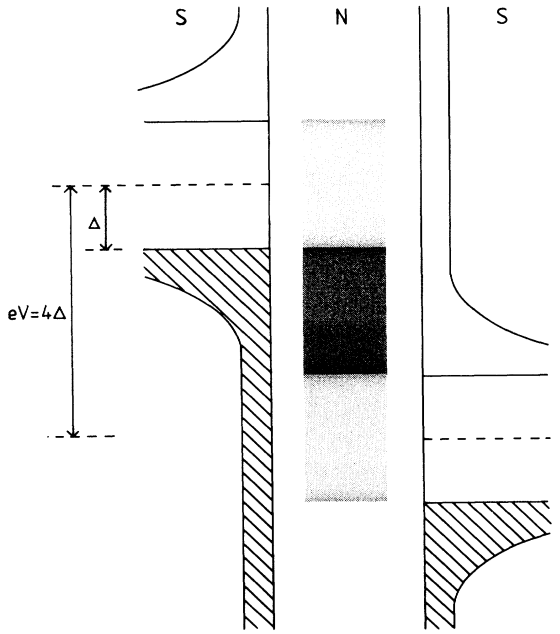

FIG. 5. Current transport through the normal region in a SINIS structure with $Z=2.0$ at $eV=4\Delta$ and $T=0$. The energy scale is plotted vertically, while the density of states in the left and right superconducting electrodes is plotted horizontally. Filled states in the electrodes are shaded. The current density in N is represented by the blackness (open: zero current, solid: high current). The high Andreev reflection coefficient at the gap edges leads to large current contributions of energy levels in N opposite the edges, just inside the gap.

opposite the edge of the gaps contribute significantly to the current. This is due to the fact that for higher Z, $A(E)$ versus E approaches a δ function with maximum value 1, peaked at $E=\Delta$.[25] The effect is clearly demonstrated in Fig. 6(a), where the individual nonequilibrium distributions are seen to be very sharply peaked at the four gap edges at $eV/\Delta=-5$, -3, -1, and $+1$. In this figure, the Fermi levels of the electrodes are placed at $eV/\Delta=0$ and -4. Note that $Z_1=Z_2$ leads to symmetric distributions: $f_{\rightarrow}(E)=1-f_{\leftarrow}(-E-eV)$.[27] The function $[f_{\rightarrow}(E)-f_{\leftarrow}(E)]$ is represented by the dotted curve and the shaded area below the curve is a measure for the current. It is interesting to compare Fig. 6(a) to the situation when the electrodes are in the normal state (the voltage is equal to the voltage applied in the superconducting state, $eV=4\Delta$). In this case $A(E)=0$, $T(E)=1/(Z^2+1)$, and $B(E)=1-T(E)$ and the following analytic solutions are easily obtained for the normal-state distributions f^N:

$$f^N_{\rightarrow}(E)=\frac{B_1T_2f_0(E+eV)+T_1f_0(E)}{(1-B_1B_2)}\ , \tag{3}$$

$$f^N_{\leftarrow}(E)=\frac{B_2T_1f_0(E)+T_2f_0(E+eV)}{(1-B_1B_2)}\ . \tag{4}$$

As shown in Fig. 6(b), these functions also represent a nonequilibrium distribution, due to the absence of scattering in N. Comparing the shaded areas below $[f_{\rightarrow}(E)-f_{\rightarrow}(E)]$ in Figs. 6(a) and 6(b), we find that the current in the superconducting state, I^S, is smaller than the normal-state current I^N. In this particular case $I^S=0.83I^N$: there is a *deficit* current in the superconducting state. This is caused by the combined presence of the superconducting energy gaps and the interface barriers. The barriers imply a small Andreev reflection coefficient, and few carriers at energy levels opposite the gaps penetrate from N into S: mostly they are reflected, effectively leading to a removal of current-carrying levels in N opposite to the gaps (cf. Fig. 5), producing a deficit current.

The situation changes drastically when interface barriers are absent. In Figs. 7(a) and 7(b) distributions are

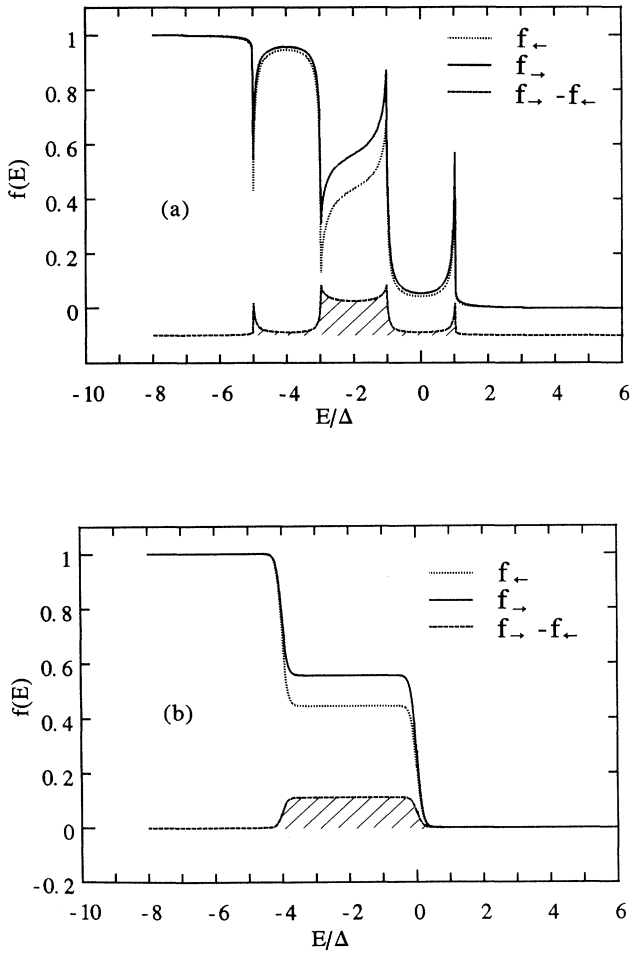

FIG. 6. Nonequilibrium distributions in N, for a symmetric SINIS junction with $Z_1=Z_2=2$, at $eV=4\Delta$ and $T=0$. (a) Superconducting state, (b) normal state. The total current is proportional to the shaded area. For clarity, the function $[f_{\rightarrow}(E)-f_{\leftarrow}(E)]$ has been displaced vertically by -0.1 in (a).

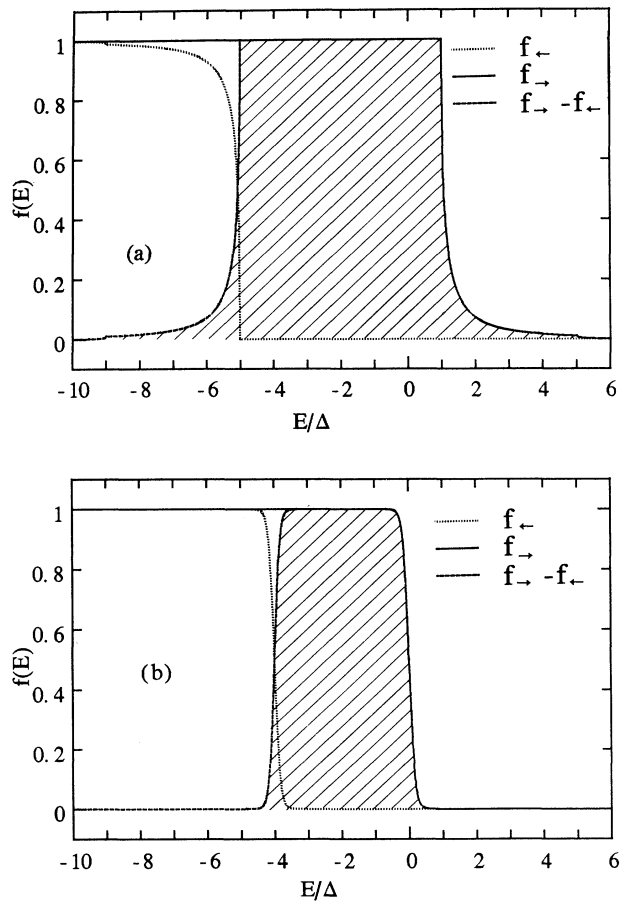

FIG. 7. Nonequilibrium distributions in N, for a symmetric SINIS junction with $Z_1=Z_2=0$, at $eV=4\Delta$ and $T=0$. (a) Superconducting state, (b) normal state. The total current is proportional to the shaded area.

plotted for $Z_1=Z_2=0$. In the normal state, the range of current-carrying energy levels in N is determined by the difference between the Fermi energies in the left and right electrode, which equals $4\Delta/e$. In the superconducting state, the range of current-carrying levels, and consequently the current through the structure, is larger. Thus, an *excess* current is present. The extra current-carrying levels are due to the fact that the Andreev reflection coefficient equals 1, for carriers at energy levels opposite the gaps, if $Z=0$. Because the Fermi levels of the electrodes are at 0 and -4Δ, the superconducting energy gaps are at energies between $-\Delta$ and $+\Delta$, respectively, -5Δ and -3Δ. In contrast to Fig. 5, where very little current flows in these two ranges, Andreev reflection leads to a large current in these ranges. Thus, the total range of current-carrying levels in N is roughly from -5Δ up to $+\Delta$. The extra levels outside this range that are shown in Fig. 7(a) reflect that $A(E)$ does not abruptly fall to zero for energies outside the gap.

A final example is shown in Fig. 8, where we plot distributions for an asymmetric junction with $Z_1=2.0$ and $Z_2=3.5$. In this case the symmetry observed in Figs. 6 and 7 is no longer present. Again, a deficit current is found.

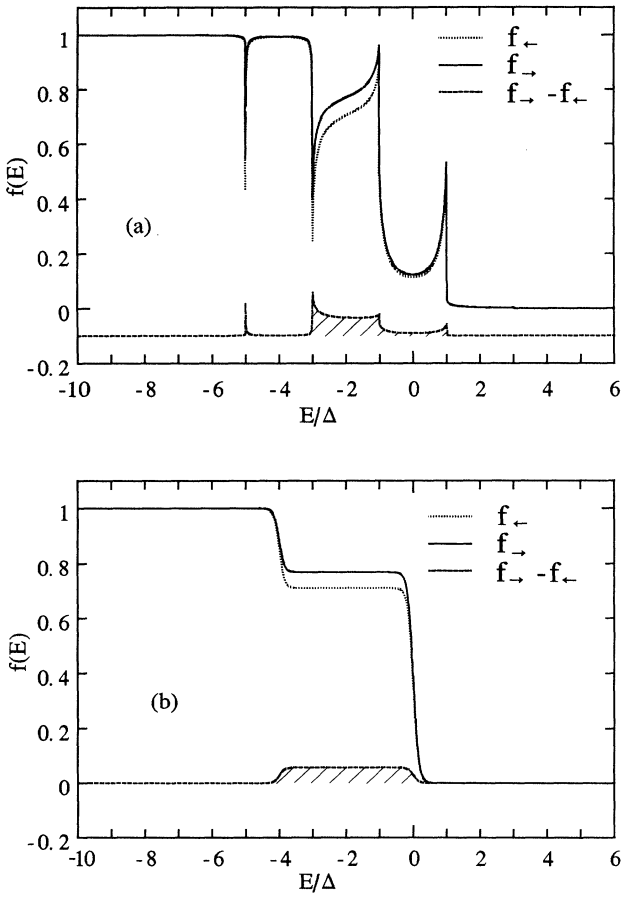

FIG. 8. Nonequilibrium distributions in N, for an asymmetric SINIS junction with $Z_1=2$, $Z_2=3.5$, at $eV=4\Delta$ and $T=0$. The total current is proportional to the shaded area. (a) Superconducting state, (b) normal state. For clarity, the function $[f_{\rightarrow}(E)-f_{\leftarrow}(E)]$ has been displaced vertically by -0.1 in (a).

From Eqs. (2)–(4) the normal-state resistance R_N can be obtained:

$$R_N=\frac{(1+Z_1^2+Z_2^2)}{2N(0)e^2v_F A}=(1+Z_1^2+Z_2^2)R_0 \ . \tag{5}$$

Together with Eq. (2), this equation allows calculation of the full current-voltage characteristic for a junction with given R_N, with $Z_{1,2}$ the only free parameters. Thus, analysis of the I,V curves in terms of the model allows the extraction of the strength of the interface barriers.

A further comparison to the model can be made through the differential resistance at zero voltage, r_0. For a single NIS junction it is given by[25]

$$r_0=\frac{R_N}{1+Z^2}\left[\int -\frac{\partial f_0(E)}{\partial E}[1+A(E)-B(E)]dE\right]^{-1} . \tag{6}$$

For $T\rightarrow 0$ this approaches the simple expression

$$r_0=\frac{(1+2Z^2)^2}{2(1+Z^2)}R_N \ . \tag{7}$$

The increase of r_0 compared to the normal-state resistance at low temperatures can be used for a quick estimate of Z for a single NIS junction. A well-known limiting case is the NIS *tunnel* junction,[28] which corresponds to Z approaching infinity. The divergence of r_0 at $T=0$ which is typical for such a junction is consistent with Eq. (7). For barriers with finite Z, the Andreev reflection coefficient $A(E)$ is greater than zero, lifting the divergence, Equation (6) predicts saturation of r_0 at lower temperatures, which can be easily understood. At higher temperatures, low voltage conduction is mainly due to tail of the equilibrium Fermi distribution in the superconductor. The tail extends to energies outside the gap, corresponding to the presence of filled states above, and empty states below the energy gap. These states contribute directly to the current. When T is lowered, the tails become smaller leading to an increase of r_0. For low enough T, the tails are much smaller than the gap and only Andreev reflection contributes to the current. The temperature dependence of $A(E)$ is governed through that of $\Delta(T)$,[25] leading to saturation of r_0.

For the SINIS system the value for r_0 is more difficult to calculate due to the diverging number of multiple Andreev reflections for $V\rightarrow 0$. Nevertheless, it is expected that the mechanism described above will also lead to saturation of r_0 at low temperatures.

B. Comparison with experiments

The characteristic features of the current-voltage characteristics discussed in Sec. II are predicted by the OTBK model. Using the results of the previous section, quantitative comparisons can be made. In Figs. 3(a) and 3(b) calculated I,V and $dV/dI,V$ characteristics at 1.2 K are shown in addition to the measurements, for $Z_1=Z_2=2.0$. The agreement is remarkably good: the

current-voltage characteristic including the magnitude of deficit current agrees well with the measurement. In the differential resistance curve the overall shape of the subharmonic gap structure is reasonably well reproduced. In obtaining the theoretical curves, the measured position of the dip at the highest voltage ($n=1$) is assumed to correspond with $2\Delta(T=1.2\ \mathrm{K})$, i.e., the structure is not shifted by heating.

The usefulness of the asymmetric model, i.e., $Z_1 \neq Z_2$, is demonstrated in Figs. 9(a) and 9(b) for a different sample. The closest symmetric fit to the 1.2-K data of the junction with area 50 μm^2 is found for $Z_1=Z_2=2.1$. For voltages below 2Δ the predicted current is too large whereas $Z_1=2.0$, $Z_2=3.5$ gives a much closer fit. Physically, the asymmetry must be related to the fact that the niobium electrodes are deposited on the silicon membrane in two separate runs. A small amount of contamination of the silicon surfaces just before deposition could easily lead to differences between the two Nb-Si interfaces and consequently, different values for Z.

A typical example of the behavior of $r_0(T)$ is shown in Fig. 10. The saturation of the zero-voltage differential resistance, discussed in the previous section, is clearly observed. The presence of this saturation in all our samples emphasizes the importance of Andreev reflection for the conduction process. Although it is valid for a single NIS junction, we have also shown the theoretical prediction expressed by Eq. (6). The overall shape of this curve agrees with the measurement.

In addition to variations of Z, we find variations of the energy gap: the value for $2\Delta(0)$ derived from dV/dI characteristics ranges between 2.6 and 2.9 meV. At the same time, the critical temperature T_c of the niobium electrodes, which is expected to be proportional to $\Delta(0)$, only varies between 8.9 and 9.0 K. The values for $2\Delta(0)$ are lower than the literature value for bulk niobium of 3.05 meV. In principle, a lowering of the gap can be caused by several processes. A large current through the structure will suppress the superconductivity in the electrodes. However, this effect is unimportant if the normal-state conductivity of the superconductors σ_S is large compared to σ_N.[29,30] This is usually the case in a semiconductor coupled weak link (in our junctions, σ_N is

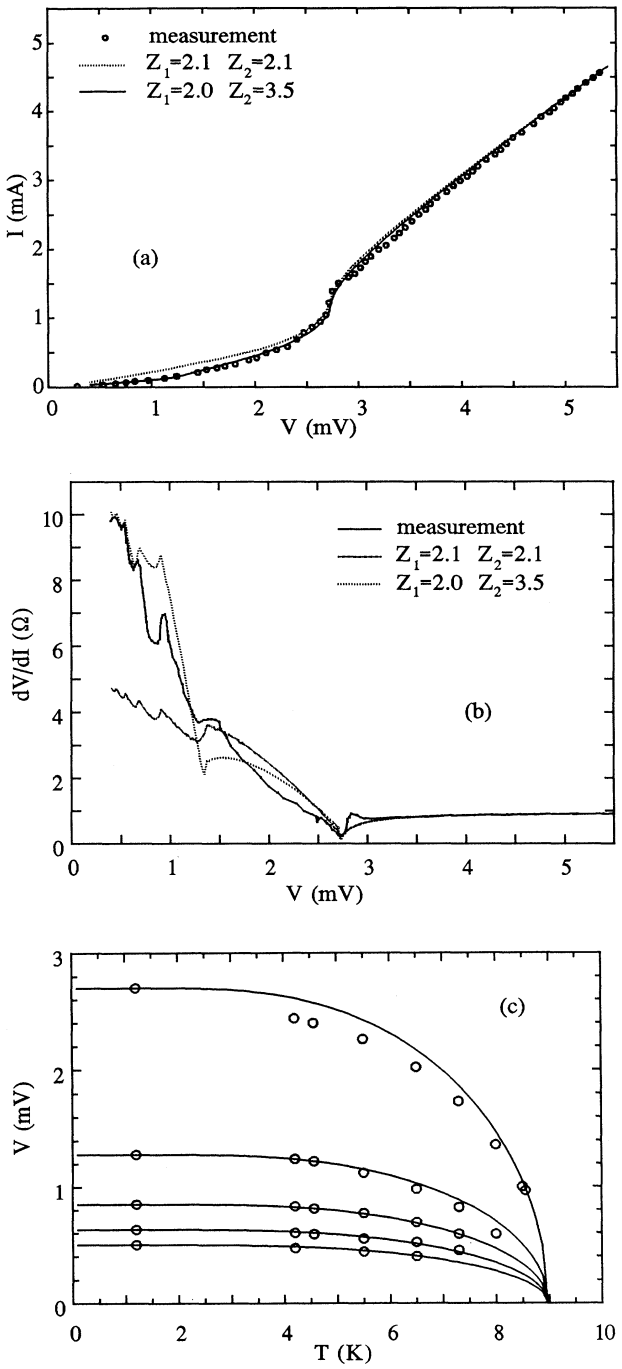

FIG. 9. (a) Current and (b) differential resistance vs voltage for a 50-μm^2 sample, at 1.2 K. Theoretical curves are calculated from the OBTK model with $Z_1=Z_2=2.1$, respectively, $Z_1=2$, $Z_2=3.5$. The temperature dependence of the subharmonic gap structure at $eV \approx 2\Delta/n$ is shown in (c).

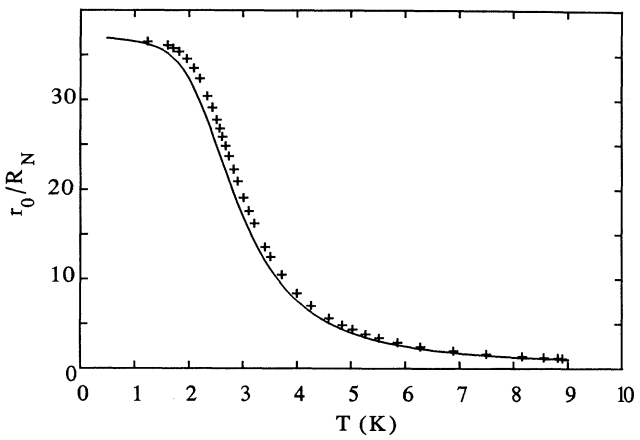

FIG. 10. Zero-voltage differential resistance r_0 as a function of temperature. For comparison, the theoretical curve for a *single* NIS junction with $Z=4.3$ is included. Qualitatively, the predicted behavior agrees with the measurement on the SINIS structure. At $T \approx T_c$, r_0 approaches the normal-state resistance, while at low temperatures saturation of r_0 is observed.

at least 2 orders of magnitude smaller than σ_S). Additionally, a strong proximity effect between S and Sm lowers the Cooper pair density, and consequently the energy gap, in S. This effect is also negligible if $\sigma_N \ll \sigma_S$.[31] We have recently confirmed the absence of a lowering of $\Delta(0)$ through measurements of the critical temperature T_c of very thin niobium films on degenerately doped Si substrates.[32] The most likely explanation for the low values for $2\Delta(0)$, together with T_c's close to the literature value of 9.2 K, is the presence of a thin disturbed Nb layer at the interfaces. Due to contamination, some intermixing of Nb and Si, strain, etc., the electronic properties of the polycrystalline niobium film at the interface could differ from the bulk properties. In the derivative measurements the density of states near the interface is probed, yielding a lowered value for $2\Delta(0)$. At the same time, the T_c measurement probes a property of the Nb electrode as a whole and yields the bulk value.

Within the OBTK model, Z determines the normal-state resistance uniquely according to Eq. (5), where A represents the conducting area. Measurements of R_N reveal that it is systematically much larger than the calculated normal-state resistance if A is identified with the geometrical area of the junction. Given the low-Z-values needed to explain the rich structure of the I,V curves, the high resistance can only be reconciled by assuming a smaller area. Apparently, only a small fraction of the interface has the high transparency implied by the Z values. For the samples discussed above, the values calculated for R_N based on the total junction area A amount to only 2–3 % of the measured value, implying an effective conducting area A_{eff} equal to $0.02-0.03\,A$.

Clearly, the superconductor-semiconductor interfaces of our junctions greatly affect their properties. The exact nature of the barriers poses an interesting question. Generally, at a metal-semiconductor interface a Schottky barrier is present. For niobium-silicon, its doping dependence has recently been studied.[33] At the high doping concentration of the present experiment, standard Schottky barrier theory[34] cannot be applied. This is demonstrated by a calculation of the barrier transmission. For Nb on heavily doped Si, transmission probabilities smaller than 0.001 are predicted by the theory. These values are contradicted by the Z values quoted above which indicate transmission probabilities 2 orders of magnitude larger. Additionally, extrapolation to the carrier concentration of the membrane implies extremely thin Schottky barriers of 3.3 nm, comparable to the spacing of the doping atoms (2.5 nm). Hence, large statistical fluctuations must be present, invalidating the use of the continuum theory.

Another factor determining the nature of the interface barrier is the possible presence of contamination. This is related to the last cleaning step of the membrane before evaporation, during which it is immersed in HF. This method, which is well known from standard silicon technology, usually leaves on the order of 0.1 monolayer of hydrocarbons on the Si surface. Detailed measurements of the position dependence of the current through a Au/Si interface[35] imply that an HF dip just before metal deposition can lead to local current variations of an order of magnitude, on a lateral scale of ≈ 10 nm. The variations are related to both submonolayer surface contamination and intermixing of Au and Si. Although our Si doping level is much higher and Nb and Si are found to intermix over only 1–2 nm,[36] these results illustrate the sensitivity to surface conditions.

Thus, it seems very reasonable to assume that the transparency of the interface barriers is strongly position dependent, which would explain our observation that only a small fraction of the interfaces is transparent. The breakdown of the Schottky barrier at high doping concentrations is an interesting problem. To study this, a superconductor-semiconductor structure is a system that supplies information not accessible by normal-metal–semiconductor contacts. Series resistance is absent in the system, and the analysis in terms of the OBTK model directly yields the transparency of the interface.

For a perfectly clean and homogeneous niobium-silicon interface the transmission will be less than unity due to the large mismatch in Fermi momentum between metal ($E_F \approx 5$ eV) and semiconductor ($E_F \approx 0.07$ eV). The Z value associated with this mismatch between two materials can be calculated from a simple equation by Blonder[37]

$$Z_{\text{eff}}^2 = Z^2 + \frac{(1-r)^2}{4r} \quad . \tag{8}$$

This equation gives the total effective barrier strength as the sum of an interface barrier of unspecified nature, with strength Z, and the effect of the materials mismatch in terms of the ratio r of the Fermi velocities. For the Nb/Si interface it implies $Z \approx 1.2$, which is slightly lower than the lowest Z of about 2 found for our samples. Equation (8) presents only a quick estimate: one cannot really conclude whether the interface transmission in the $Z=2$ sample is limited by Fermi momentum mismatch only, or if additional scattering is present. Nevertheless, the orders of magnitude agree, and the large difference in E_F quoted above is representative for most metal-semiconductor combinations. Hence, it can be concluded that in SSmS heterostructures momentum mismatch results in an intrinsic barrier that significantly influences the current-voltage characteristic. Additionally, it will have an important effect on the supercurrent.

C. Temperature dependence

Given the good quality of the fits to the SINIS model at 1.2 K, an unambiguous description of sample behavior at higher temperatures should be possible, using the 1.2-K values for Z. As we will show, self-heating plays an important role at higher temperatures, making a direct application of the model difficult. Additionally, inelastic scattering may be present, further complicating the analysis at elevated temperatures.

The temperature dependence of the position of the dips in the differential resistance of the asymmetric sample discussed above is displayed in Fig. 9(c) (dots). The OBTK model predicts the position of the dips to behave with temperature as $\Delta(T)$. In Fig. 9(c), the measured position of each individual dip is therefore compared with the standard BCS temperature dependence of the gap, as-

suming the position of each dip at 1.2 K to be unaffected by heating. The behavior is similar to that of the symmetric sample, shown in Fig. 3(c). The structure at $eV=2\Delta$ is much more shifted towards lower voltages than the higher-order dips. A likely cause for this is heating of the sample due to the power dissipated by the dc measuring current. This idea is supported by measurements such as shown in Fig. 11, for the symmetric ($Z=2$) sample. In other samples similar behavior is observed. At 4.2 K the shifted position of 2Δ corresponds to $T=5.8$ K, implying a temperature rise of 1.6 K at $eV=2\Delta$. Moreover, the measured I,V characteristic lies above the theoretical curve for eV higher than 1–1.5 mV, also implying an increase of the temperature. The theoretical curve is calculated using the Z values inferred from the fit to the SINIS model at 1.2 K. Between 3.5 and 4 mV there is a kink in the I,V curve, corresponding to an increase in the differential resistance of about 0.4 Ω. From separate measurements we know this corresponds to the added resistance of the electrodes: the niobium undergoes a superconducting-normal transition at the kink. At voltages slightly above 2Δ, the dV/dI characteristic becomes noisy, presumably because the power dissipated is sufficient to cause locally active boiling of the He bath.[38,39]

Below the λ point of helium, $T=2.17$ K, the noise completely disappears in all the samples. Additionally, the kink disappears or shifts to much higher voltages. These phenomena are caused by superfluid transition of helium at 2.17 K. Below this temperature the heat transfer from the sample to the bath is greatly improved.[38]

From the above observations, we conclude that the voltage axis in Fig. 11 can also be considered a temperature axis, increasing from $T=4.2$ K at $V=0$ to $T=T_c$ at 3.7–3.8 mV. Consequently, the I,V curve cannot be described by a simple model calculation for 4.2 or 5.8 K. We can attempt, however, to estimate the magnitude of heating effects.

In the SINIS model, carriers originating from the left superconductor with energy E traverse the normal region

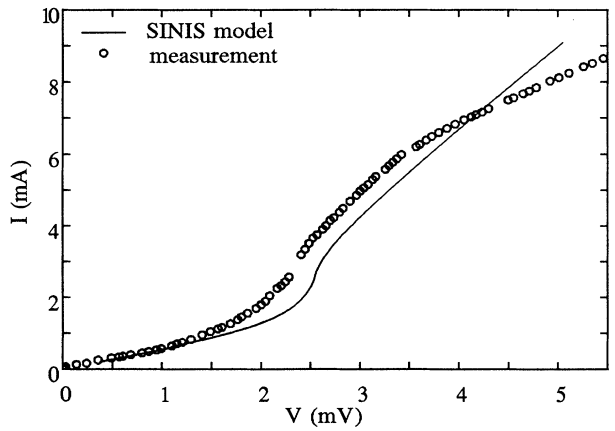

FIG. 11. Current-voltage characteristic of the $Z_1=Z_2=2$ sample (Fig. 3) at 4.2 K. The kink at 3.5–4 mV is due to the superconducting-normal transition of the niobium electrodes.

to arrive as "hot" electrons in the right superconductor with energy $E+eV$, where they will dissipate their extra energy. An upper limit to the temperature rise due to heating can be calculated by assuming (1) all the heat is generated in a Nb film of the same size as the window in the Si_3N_4 layer (Fig. 1), and (2) direct heat transport from this film to the He bath is negligible due to the high thermal boundary resistance between liquid He at 4.2 K and a metal. The temperature increase δT due to heat flow P through an interface with area A and thermal boundary conductivity α is $\delta T=P/\alpha A$.[40] We estimate the value of α for Nb-Si to be 1.6 W/K cm^2 at 4.2 K, based on Kaplan's theory for the acoustic mismatch between solids.[41] Although this is only a crude estimate, the order of magnitude is in agreement with values found for other superconductor-substrate boundaries from heating in microbridges.[38,42–43] From this α, together with $P=V\times I=9$ μW and the junction area 35 μm^2, we find $\delta T=16$ K for $eV=2\Delta$, at 4.2 K.

For an estimate of the lower limit to the expected temperature rise we also take into account thermal conduction within the niobium film. The combination of heat transfer across the boundaries and thermal conduction leads to a characteristic thermal healing length r_T along the film, $r_T=(\kappa t/\alpha)^{1/2}$, with κ the thermal conductivity of the film and t its thickness.[42] With $\kappa=0.2$ W/cm K (Ref. 44) we find $r_T=19$ μm. This value implies that heat is transferred across the Nb film boundary from a much larger area than the 35 μm^2 used above. From the estimated upper value of about 1900 μm^2 for this area, $\delta T\approx 0.3$ K is found, which can be regarded as a lower limit. This limit might be decreased due to heat transport directly across the film boundary into the He bath. To calculate the contribution of this process, the value of α(Nb-He) is required. To our knowledge there are no measurements of this parameter at $T>2.17$ K. Decker[42] mentions α(metal to helium)≈ 0.01 W/cm^2 K at $T=3$ K. Comparing this order of magnitude to the value for Nb-Si estimated above, it seems justified to neglect heat flow from the Nb film into the bath.

We stress that these limits are order-of-magnitude numbers due to the large uncertainty in parameter values and the complicated geometry. The estimate of r_T neglects that on one side of the membrane, outside the window in the insulating layer, the Nb film has a Si_3N_4 film as its neighbor rather than silicon (cf. Fig. 1). In addition to this, a thin disturbed niobium layer at the interfaces might lead to additional thermal resistance, effectively decreasing α(Nb-Si).

An independent check can be made by estimating the voltage at which the superconducting-normal transition should take place from the known temperature rise at $eV=2\Delta$. From Fig. 11 it is known that the temperature rise $\delta T=1.6$ K corresponds to $P=9$ μW. In order to reach a T_c of about 9 K by self-heating, a temperature rise of 4.8 K above the bath temperature is needed. This requires $P=(4.8/1.6)\times 9$ μW$=27$ μW (assuming that thermal conductivities do not change too much in this temperature range). According to Fig. 11, $P=27$ μW corresponds to a voltage of about 3.9 mV which is close to the position of the kink.

We conclude that self-heating due to the dc measuring current distorts the I, V characteristics. The presence of heating is indicated by a number of experimental results. The temperature rise inferred from the I, V curves is not contradicted by rough estimates for upper and lower limits from simple model calculations. A realistic, quantitative analysis is difficult due to the complicated geometry and the uncertainty in the thermal boundary resistances.[45]

D. Inelastic scattering

From the measurements shown in Figs. 12 and 13, rather high interface barriers are inferred. As we will demonstrate below, this may lead to a relatively large influence of inelastic scattering. The measurements are not very well described by the symmetric OBTK model. Below $eV=2\Delta$ the wrong curvature is predicted by the model. Especially below $eV=\Delta$ the calculated differential resistance is much too low. Although the asymmetric fit is not as good as in previous figures, improvement is obtained compared to the symmetric prediction: a large increase in dV/dI at low voltages is implied. Theoretical curves for $Z_1=2.5$ and $Z_2=5.6$ are shown, but comparable fits are obtained for slightly higher Z_2.

We consider the possibility that the lesser quality of the fits in Figs. 12 and 13 is due to the presence of inelastic scattering. In Ref. 20, the inelastic-scattering length in heavily doped n-Si is found to be 0.4 μm at 1.2 K, 0.18 μm at 2.4 K, and 0.1 μm at 4.2 K. These values imply that at temperatures above a few K inelastic scattering becomes increasingly important. A simple model to investigate the influence of inelastic scattering in the normal metal in a SINIS structure has recently been presented.[17] High-Z values are assumed at the interfaces, effectively suppressing Andreev reflection. Inelastic scattering is taken into account through a relaxation model. Carriers are injected from the left superconductor into N at a rate Γ_B. In N, there is competition between extraction of the carriers into the right superconductor at rate Γ_B and energy relaxation towards the equilibrium distribution at rate $1/\tau_E$. τ_E is assumed not to depend on energy or on the degree of nonequilibrium. The injection or extraction rate Γ_B is defined as

$$\Gamma_B=\frac{1}{N(0)e^2R_cL} \tag{9}$$

with the R_c the contact resistance and L the thickness of the normal layer. Within the context of the OBTK model, R_c equals $R_N A/2$ with A the junction area. If Γ_B is smaller than about $0.01/\tau_E$, relaxation dominates and the equilibrium Fermi distribution is present in N. However, if $\Gamma_B > 10/\tau_E$, a strong nonequilibrium distribution is present in N, leading to a reduced subgap current and a current deficit. The latter result is analogous to that of the OBTK model for high Z. For values between about 0.01 and 10, the degree of nonequilibrium in N increases rapidly with $\Gamma_B\tau_E$. Thus, $\Gamma_B\tau_E$ is a measure for the degree of nonequilibrium in N.

Using τ_E from Ref. 20 and the effective conducting area A_{eff} (obtained as discussed in Sec. III B), we estimate $\Gamma_B\tau_E \leq 40$ at 1.2 K and ≤ 2 at 4.2 K for the sample of Figs. 12 and 13. These values imply that at 4.2 K the sample is not in the strong nonequilibrium range, but rather in the intermediate range, where the temperature dependence of τ_E strongly influences the distribution in N. An additional indication for this is the fact that the measured I, V characteristic at 4.2 K lies entirely above the theoretical curve. This behavior is predicted by the model of Ref. 17. As was shown there, increasing inelastic scattering for a given Γ_B results in an upward shift of the I, V curve, towards the equilibrium curve (with zero deficit current) for 2 NIS tunnel junctions connected in series. Due to the relatively high barriers, the I, V curve at 1.2 K might also be affected by inelastic scattering. Although this idea seems to be contradicted by the $\Gamma_B\tau_E$ value calculated above, it is supported by the absence of subharmonic gap structure with $n \geq 3$. Due to the increasing number of traversals of the silicon, higher-order SGS will be increasingly weakened by inelastic scattering. The values used for τ_E used in this section have been ob-

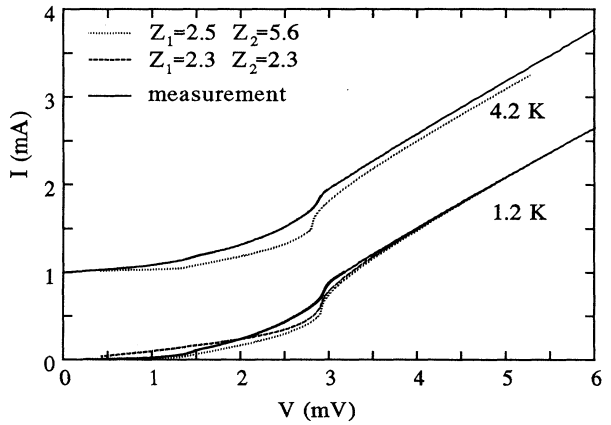

FIG. 12. Current-voltage characteristics of a 48-μm^2 sample at 1.2 and 4.2 K. Theoretical curves are obtained from the OBTK model. At 4.2 K, the upward shift of the measured I, V curve at high voltages may be indicative of inelastic scattering.

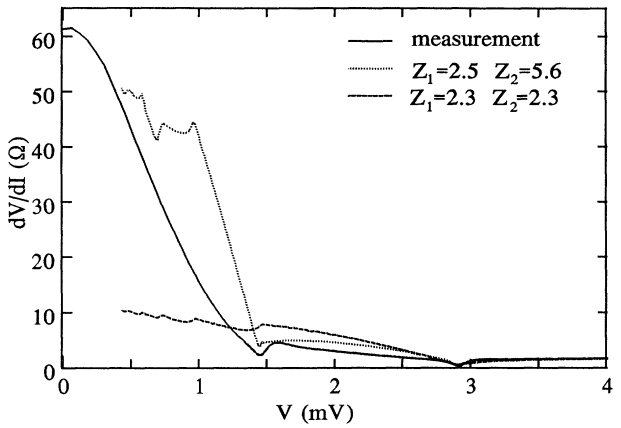

FIG. 13. Differential resistance vs voltage for the junction from Fig. 12, at $T=1.2$ K.

tained for n-type silicon rather than p-Si, hence the numbers in this analysis should be taken as an indication for the strength of the effect only.

It is interesting to note that, contrary to other samples, in Fig. 12 no direct evidence for heating is found: the voltage corresponding to 2Δ at 4.2 K is consistent with the BCS behavior of $\Delta(T)$ within about 0.1 K. Comparison to other samples shows that this is not completely due to the lower power P dissipated: at $eV=2\Delta$, P equals $\frac{1}{4}$ of the power dissipated in the sample shown in Fig. 11. As the junction areas are roughly equal, a temperature rise of a few 0.1 K would be expected. Possibly, inelastic scattering in the silicon leads to transfer of the carrier energy to the phonon gas in the membrane, instead of to phonons in the electrodes (cf. Sec. III C). Thus, the excess energy flows easily away from the junction region into the surrounding bulk of the chip, rather than across the interfaces into the electrodes, causing no gap depression.

For a more quantitative approach to inelastic scattering in a SINIS structure it would be very useful to integrate the relaxation model with the OBTK description. A first step towards this goal was recently presented by Nitta *et al.*[46] for the case of $Z=0$, i.e., absence of interface barriers. For this case, which can be solved analytically, strong smearing of higher-order SGS is predicted. Comparable results have been obtained by Kümmel, Gunsenheimer, and Nicolsky[47] for SNS junctions without interface barriers, using a different approach. The authors solve the time-dependent Bogoliubov–de Gennes equations in terms of wave packets describing the carrier motion and obtain I,V characteristics containing subharmonic gap structure and an excess current. The behavior predicted for increasing $\Gamma_B\tau_E$ is similar to that observed in Figs. 12 and 13: the subgap structure is smeared by inelastic scattering, and at high voltages the I,V curves move towards the equilibrium characteristic.

E. Silicon Fermi level

In addition to temperature-dependent effects, the band structure of the intermediate silicon could, in principle, complicate the SINIS model analysis of the junctions. In the model, the density of states of the intermediate material is assumed to be structureless. This is justified by comparing the Fermi energy E_F to the voltage range of interest. E_F is defined as the energy difference between the valence band edge and the Fermi level of the degenerate silicon. Based on simple free-electron parameters, we calculate $E_F=71$ meV, implying that for voltages of a few millivolts the density of states is essentially constant. E_F is calculated from two parameters: the density-of-states effective mass $m_d^*=0.87$ and the carrier concentration $n=7\times10^{19}$ cm^{-3}. Effective masses are discussed in some detail in Sec. IV B. The average concentration n is derived from the doping profile shown in Fig. 14. The profile is generated by SUPREM III, a simulation program for semiconductor processing.

An experimental determination of E_F should be possible through the measurement of the differential resistance

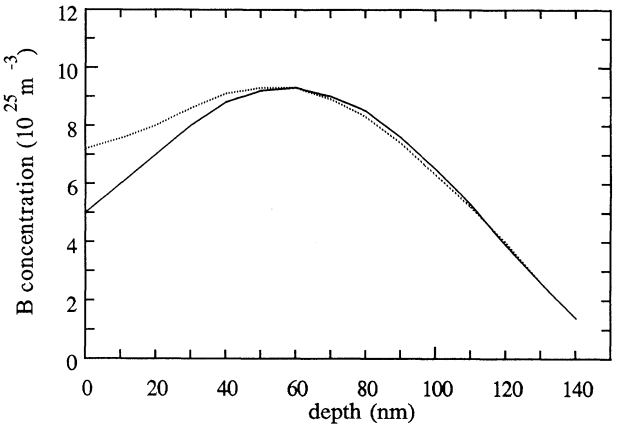

FIG. 14. Doping profile in silicon before membrane etching. The profile is obtained using SUPREM III to model the low-energy implantation used plus the subsequent anneal at 800 °C. Solid curve: anneal in the presence of a 2–3-nm silicon dioxide surface "capping," dotted curve: anneal without capping.

for voltages on the order of a few times E_F/e. In analogy to tunneling measurements,[28] a maximum in dV/dI is expected when the voltage drop over one NS interface is equal to E_F. Consequently, in a junction with V equally distributed over both interfaces the maximum will occur at $eV=\pm2E_F$, neglecting a possible voltage drop over the bulk silicon. For a strongly asymmetric junction, such as the one discussed in the previous section, the situation changes drastically. For negative V, the maximum should occur at V slightly higher than E_F, while for the opposite polarity it occurs at $eV\gg2E_F$ (Fig. 15). The polarity of V corresponds to the top surface of the sample (Fig. 1). Thus, measurements at relatively high voltages are expected to confirm the presence of asymmetry that was originally inferred from low voltage measurements.

This is illustrated by Fig. 16, in which we show the asymmetric characteristic found for the sample discussed

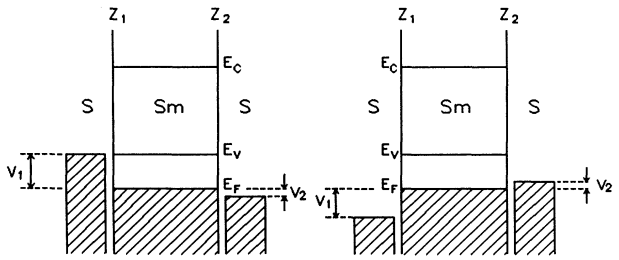

FIG. 15. Voltage drop in an asymmetric SSmS system. The energy is plotted vertically, the density of states horizontally. On the energy scale shown, the density of states is taken to be constant. Shading indicates filled states. In the intermediate p-type semiconductor, the conduction band edge, valence band edge, and Fermi level are indicated by E_C, E_V, and E_F. Because $Z_1\gg Z_2$, most of the applied voltage $V=V_1+V_2$ drops at the left interface. In the left picture a negative voltage is applied to the left electrode and a maximum in dV/dI occurs because the Fermi level of the left electrode is opposite E_V. In the right picture the polarity is reversed and the maximum will occur for voltages much greater than (V_1+V_2).

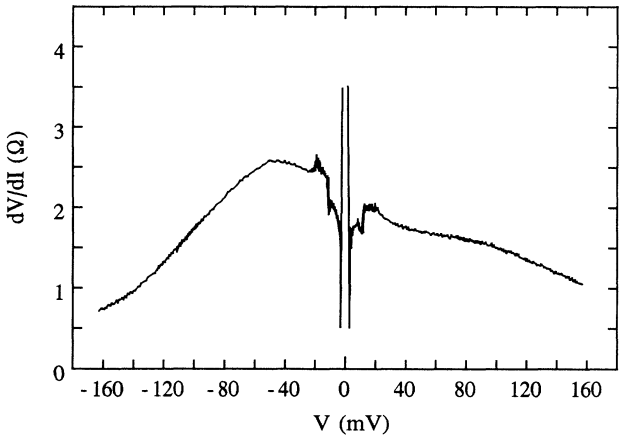

FIG. 16. Differential resistance at high voltages. The structure close to $V=0$ is due to the superconductivity of the niobium. The maximum at ≈ -50 mV corresponds to the Fermi level of the semiconductor.

in the previous section. For V relatively close to zero, structure due to the superconductivity of the niobium electrodes is present. At $eV \approx 10$ mV there is a noisy superconducting-normal transition. As discussed above, there is no indication for the presence of heating in the junction itself. Thus, the transition is presumably caused by localized heating on the chip some distance away from the junction. Its origin lies probably in the series resistance at the electrical contacts to the chip, which are made through springcontacts pressed onto its top and bottom surfaces. Above the superconducting-normal transition, the structure in dV/dI is related to the properties of the semiconductor. Taking into account the Z values for the sample, the maximum present at about -50 mV corresponds to a Fermi energy of ≈ 42 meV, for the top surface.

This value is significantly lower than the calculated value of 71 meV. The latter value would be too large if the actual carrier concentration were lower than the concentration derived from Fig. 14. However, $E_F = 42$ meV corresponds to $n \approx 2.6 \times 10^{19}$ cm^{-3} which is unrealistically low: the etchant used to produce the membrane (cf. Sec. II) does not stop at boron concentrations below $5-6 \times 10^{19}$ cm^{-3}.

The calculated E_F wold also be too large if the effective mass were taken too small. However, to obtain $E_F = 42$ meV, $m_d^* = 1.47$ is required which is an unrealistic value for degenerate p-Si. Moreover, the calculated E_F is confirmed by tunneling measurements by Cullen, Wolf, and Compton.[48] Their Fermi energy versus boron doping measurements on degenerately doped silicon indicate $E_F = 70-80$ meV for $n = 7 \times 10^{19}$ cm^{-3}, in agreement with our value.

These considerations lead to the conclusion that what is measured must be the Fermi level close to the top silicon surface, instead of the average bulk value. This implies a relatively low boron surface concentration. This might be due to outdiffusion: during the high-temperature step (800 °C) of the fabrication process the dopant escapes from a very thin surface layer of the silicon wafer. Outdiffusion is not very well characterized: profile measurements are rather unreliable very close to the surface and the boron profiles found in the literature are not always consistent with each other. In some cases secondary ion mass spectroscopy (SIMS) seems to indicate a relatively low dopant concentration, after an anneal comparable to ours, close to the surface.[49] The presence of a native oxide of 2–3 nm on top of the silicon wafer during the anneal poses an additional complication. Thus, the exact behavior of the dopant very close to the surface is difficult to predict. The significance of outdiffusion could be tested by annealing without a native oxide. Because diffusing boron atoms prefer silicon dioxide to silicon, this should result in less outdiffusion (illustrated in Fig. 14) and, consequently, a higher Fermi energy.

The difference in boron surface concentration implies an intrinsic asymmetry in the junctions. However, Eq. (14) implies a difference in Z between top and bottom interfaces of only 25%, which is small compared to the values found in practice. Consequently, this difference plays only a minor role in determining the asymmetry of the junction.

IV. SUPERCURRENT BEHAVIOR

The key results of Sec. III are that the SSmS structure studied is a mesoscopic system, and that its behavior in the voltage-carrying state is to a great extent determined by the barriers at the superconductor-semiconductor interfaces. Both findings have important consequences for supercurrent transport.

The mesoscopic character leads to the observation that, in principle, two parallel channels for supercurrent transport are present. The first one is described by conventional theory for superconductivity in nonhomogeneous systems. In systems with the elastic-scattering length l of the intermediate normal layer much smaller than its thickness the theory is usually expressed by the linearized form of the Gorkov equations[50] or by the Usadel equations.[51] The corresponding physical picture is that of the proximity effect: the pair correlation between electrons present in the superconductors diffuses over a characteristic length into the intermediate material. In clean systems, the Bogoliubov–de Gennes equations[52] are often used to calculate I_c. Phase coherent supercurrent transport through a clean normal metal has been studied around 1970 by Kulik[4] and Bardeen and Johnson.[5] Assuming unity Andreev reflection probability at the NS interfaces, constructive interference between Andreev reflected electrons and holes was found to lead to formation of bound states carrying the supercurrent through the normal metal. Technological progress with high-mobility semiconductors and mesoscopic structures has recently led to an extension of these ideas. The excitation spectrum in N has been calculated using a Green's function technique,[7] a scattering matrix formalism originally used for electron transport in normal metals and semiconductors,[6,8] or a relaxation time model.[9] Although these two physical pictures for supercurrent transport look rather different, they represent two limiting cases

(diffusive transport or ballistic transport) of the same underlying theory.

The second channel for the supercurrent is based on weak localization effects in the intermediate layer.[53] Adding contributions of different phase coherent scattering paths and taking into account phase shifts due to Andreev reflection a supercurrent is found which is fundamentally different from the first channel. We discuss this current component in Sec. IV B.

The elastic length in the silicon is about 5 nm, which is much smaller than the membrane thickness $L=50$ nm. Consequently, carrier transport is diffusive in the system and it is expected that the supercurrent is adequately described in terms of the Usadel equations (taking into account the presence of interface barriers). Additionally, there might be a contribution due to weak localization effects.

A. Proximity effect

1. *Kupriyanov-Lukichev theory (Ref. 15)*

After the pioneering work of de Gennes[1] in the 1960s many theories for the supercurrent through a normal-metal-coupled weak link have been proposed. Most of these have a restricted range of validity, due to one or more of the following assumptions that have been made. (1) The normal-state parameters of N and S are identical. (2) The transmission of the NS interface equals unity. (3) The temperature is very close to T_c. (4) The thickness of N is either very large or very small compared to ξ_N. The coherence length ξ_N is defined below in Eq. (10).

Recently, Kupriyanov and Lukichev proposed a theory for the critical current through SNS and SS'S junctions that is not subject to the above restrictions.[15] As we will show, it is especially suited to describe semiconductor coupled weak links. The authors have used the general Eilenberger equations in the immediate vicinity of the interface to find boundary conditions at the SN or SS' interface, valid at any temperature and at any interface transmission. Solving the Usadel equations, the critical current through the weak link has been obtained for arbitrary temperature, interface transmission, and normal-state parameters. To arrive at this result, the suppression of superconductivity in the electrodes due to the proximity effect and the current through the structure are assumed to be small. As we have argued in Sec. III B, these assumptions are valid for the present experiment due to the large difference in resistivity between Sm and S.

Due to the inclusion of interface barriers of arbitrary strength, the Kupriyanov-Lukichev (KL) theory treats a SINIS structure, rather than a SNS structure. This makes it also well suited to describe SNS junction based on high-T_c materials, in which interface barriers are often present.[54]

The theory is valid in the dirty limit, in this case defined through the condition $l \ll \xi$, with l the elastic mean free path. The normal-metal coherence length ξ_N is an important parameter determining the magnitude of I_c in many proximity effect theories for the critical current in SNS weak links. It represents roughly the depth over which the pair correlation penetrates into N and is given by

$$\xi_N = \left[\frac{\hbar D}{2\pi kT} \right]^{1/2} \tag{10}$$

with diffusion constant $D = v_F l/3$ and v_F the Fermi velocity. For future use, we write Eq. (10) in terms of semiconductor parameters to obtain ξ_{Sm}.[55] Based on a free-electron model, v_F can be obtained from the carrier concentration n, density-of-states effective mass m_d^*, and valley degeneracy v:

$$v_F = \frac{\hbar}{m_d^*} \left[\frac{3\pi^2 n}{v} \right]^{1/3} . \tag{11}$$

The elastic mean free path is determined by the conductivity effective mass m_c^* and the drift mobility μ:

$$l = v_F \tau_{\mathrm{el}} = \frac{m_c^* \mu v_F}{e} . \tag{12}$$

In the last two equations, a distinction is made between effective masses, corresponding to different physical aspects of the semiconductor. The density-of-states effective mass is relevant for calculating the Fermi energy and related quantities, whereas the conductivity effective mass is required for transport phenomena. Substituting Eqs. (11) and (12) in Eq. (10), the semiconductor coherence length (in the 3D case) is expressed as

$$\xi_{\mathrm{Sm}} = \left[\frac{\hbar^3 m_c^* \mu}{6\pi e k T m_d^{*2}} \right]^{1/2} (3\pi^2 n/v)^{1/3} . \tag{13}$$

As will be discussed in Sec. IV A 3, this expression differs importantly from expressions for the coherence length used previously.

In KL theory, the magnitude of I_c is determined by the interface transmission and the normal-metal (or semiconductor) coherence length. These two quantities are parametrized through the dimensionless Γ, which is equal to the ratio of the interface resistance to the bulk resistance of the intermediate material, and $\beta_\omega(T)$ which is defined as

$$\beta_\omega(T) = \frac{L}{2\xi(T_c)} \left[\frac{\omega}{\pi k T_c} \right]^{1/2} \tag{14}$$

in which the Matsubara frequency ω is defined as $\omega = (2n+1)\pi kT$, $n = 1,2,3$. The expression for the critical current is

$$I_c(T) = \frac{4\pi kT\Delta(T)^2}{eR_N} \sum_\omega \frac{\beta_\omega(1+2\Gamma)}{[\omega^2+\Delta(T)^2][(1+4\Gamma^2\beta_\omega^2)\sinh(2\beta_\omega)+4\Gamma\beta_\omega\cosh(2\beta_\omega)]} \tag{15}$$

when the boundary transparency is not too large. This "small transparency limit" is defined through

$$\frac{\Delta(T)}{\pi kT} \ll 1+2\beta(T)\Gamma\tanh[\beta(T)] \ . \tag{16}$$

Equation (15) represents a very general expression for the critical current through a SNS or S-Sm-S system. Several well-known equations that have been obtained earlier can be derived from it as limiting cases. For T very close to T_c the condition expressed by Eq. (16) is also met for large boundary transmission, and in this limit Likharev's result for SNS variable thickness bridges[56] can be rederived, as well as de Gennes' expression for I_c.[1] For T approaching zero the condition cannot be satisfied and I_c has to be found numerically instead of through Eq. (15).

2. Comparison with experiments

We compare our measurements with Kupriyanov-Lukichev theory. In Fig. 17, the critical current I_c is shown as a function of temperature T, for two junctions with area A of 120 and 150 μm^2 (hereafter referred to as $S1$ and $S2$, respectively). The supercurrent persists up to the critical temperature of the niobium electrodes and increases rapidly when T is lowered. The predictions of the KL theory are shown as solid curves. The measurements are very well described by the theory over the whole temperature range. The theoretical curves are obtained from Eq. (15) by adjusting the values of both $L/\xi(T_c)$ and Γ. The following values are found for $S1$: $\Gamma=79$, $L/\xi(T_c)=2.4$, and for $S2$: $\Gamma=85$, $L/\xi(T_c)=2.3$. Fits of almost equal quality are obtained for $L/\xi(T_c)$ differing ± 0.1 from these values. The corresponding Γ's are about 10% larger or smaller. In this parameter range, Eq. (16) is satisfied at all temperatures of the measurement, confirming the validity of the approach. Below about 0.5 K, Eq. (16) is no longer satisfied. For the β and Γ values reported above, the temperature dependence of the critical current is contained exclusively in the parameter $\beta(T)$, whereas the magnitude of I_cR_N scales with $1/\Gamma$. Hence, a large boundary resistance implies a strong reduction of the I_cR_N product of the junction.

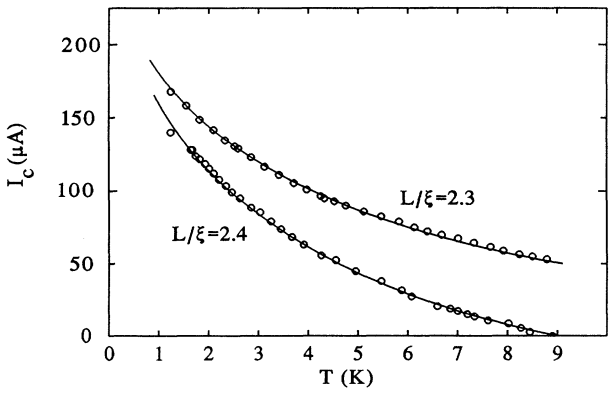

FIG. 17. Critical current vs temperature for two different samples (dots) together with predictions of Kupriyanov-Lukichev theory (solid curves, see text). For clarity, the $L/\xi=2.3$ data and predictions have been displaced upwardly by 50 μA.

The analysis of the voltage-carrying state presented in Sec. III offers the interesting possibility of an independent estimate of Γ. From the I,V characteristics of $S1$ and $S2$, we estimate $Z_{1,2}\approx 2.5$ and 3 for both samples. The resistance due to the interface barriers can be calculated from Eq. (5). Dividing this by the bulk resistance of the membrane R_b, estimated from $R_b=\rho L/A$ yields Γ. For both samples a Γ value of about 1 is found, evidently much smaller than the values obtained above. The $I_c(T)$ data of Fig. 17 cannot be fitted to the Kupriyanov-Lukichev expression, Eq. (15), with Γ values on the order of unity. This is not surprising, as these values are outside the small transparency limit.

Some insight in the discrepancy between the different Γ's is obtained from the observation that the calculated interface resistance is much smaller than the measured normal-state resistance R_N. As discussed in Sec. III, the relatively large values for R_N reflect the fact that only a small fraction of the interface is transparent. The interface is pictured as an opaque separation between S and Se, with many small transparent spots connecting both materials. After being injected in the membrane the current fans out, leading to a bulk resistance smaller than the value based on the areas of the individual transparent spots. The lower limit to the bulk resistance resulting from this is determined by the total area A of the junction. The corresponding upper limit to Γ is R_N/R_b, which is on the order of 75. Taking into account the uncertainties in Γ determined from Fig. 17 and in the other parameters relevant for these calculations, L and ρ, this value is in reasonable agreement with values obtained from KL theory. Stated differently, the Γ's inferred from both methods agree if the interface resistance is determined by the area of the transparent spots only while at the same time the current is carried by the total area A of the junction.

Next we compare the coherence lengths found above with the theoretical values. For a membrane thickness between 40 and 60 nm, the L/ξ values found imply $\xi_{Sm}(T_c)\approx 21\pm 5$ nm. From Eq. (13), we obtain the value $\xi_{Sm}(T_c)=6$ nm. The disagreement of a factor 3.5 between these values is significant. The values used for the carrier concentration, mobility, and effective mass to calculate ξ are discussed in some detail in the Appendix. Although there are some uncertainties in the parameters n and μ, they are much too small to account for the large discrepancy. A possibility is that the use of a simplified band-structure model[57] for the (100) silicon crystal of the present experiment is fundamentally in error. The complicated band structure of p-Si is roughly approximated by the use of effective masses, obtained by averaging over three hole masses that correspond to the three different hole bands in p-Si. A detailed analysis of the relation between band-structure and transport properties may be required to clarify the discrepancy.

Perfect agreement with the KL analysis is obtained if the effective masses were determined completely by the lowest value known: substituting the low doping light hole mass $m_l=0.153$ in Eq. (13) yields $\xi_{Sm}=20.3$ nm. Substitution of the lowest effective mass for the high doping used in our experiment, the split-off mass $m_{so}=0.234$

yields $\xi_{Sm}=16.5$ nm, in reasonable agreement with KL. However, there is no physical argument justifying substitution of either value.

3. *Previous theories*

In previous experiments on SSmS junctions, agreement between the theoretical coherence lengths and values for ξ inferred from $I_c(T)$ has invariably been reported. At this point it is clarifying to compare the present analysis with the theories that have been used previously to interpret supercurrent behavior.

In the literature on semiconductor coupled weak links, $I_c(T)$ measurements are usually analyzed in terms of the well-known model for SNS junctions of Likharev[29,55] or the SSmS model of Seto and van Duzer.[3] The latter authors obtain the following expression for the supercurrent through a semiconductor with length L:

$$I_c(T)\propto\left[\frac{\Delta(T)}{\cosh[L/2\xi_{Sm}(T)]}\right]^2\frac{L}{\xi_{Sm}(T)}\ . \tag{17}$$

Here $\Delta(T)$ is the energy gap of the superconductor. Most systems studied to date are long junctions, i.e., $L\gg\xi$, for which Eq. (17) simplifies to

$$I_c(T)\propto\Delta(T)^2\frac{L}{\xi(T)}\exp[-L/\xi(T)]\ . \tag{18}$$

The expression found by Seto and van Duzer for the coherence length is

$$\xi_{Sm}=\left[\frac{\hbar^3\mu}{6\pi ekTm^*}\right]^{1/2}(3\pi^2n)^{1/3}\ . \tag{19}$$

This equation differs from our expression for the coherence length, Eq. (13), in two aspects: the distinction between the effective masses m_c^* and m_d^* has been neglected, as well as the possibility of a nonunity valley degeneracy v. This is only correct for n-type III-V compounds. For Si, Ge, and p-type III-V semiconductors, $v\neq1$ and/or $m_c^*\neq m_d^*$. Nevertheless, Eq. (19) or its 2D equivalent has been used in virtually every analysis of semiconductor-coupled weak-link measurements reported to date. For completeness, we note that in two dimensions the complete expression for the coherence length is

$$\xi_{Sm}=\left[\frac{\hbar^3\mu m_c^*n_s}{2ekTm_d^{*2}v}\right]^{1/2} \tag{20}$$

with $D=v_Fl/2$, $k_F=(2\pi n_s)^{1/2}$, and n_s the sheet carrier concentration.

Next we take a critical look at the Seto–van Duzer analysis of the critical current. It is much less sophisticated than KL: the influence of the NS boundaries is not treated at all and the theory is based on the lowest Matsubara frequency only. Furthermore, Eq. (17) is based on results of de Gennes[1] which are obtained using Ginzburg-Landau (GL) theory. The Ginzburg-Landau equations are valid for small values of Δ, so Eq. (17) is only valid near T_c. The induced pair correlation in the semiconductor might also be small at lower temperatures, so the range of validity could, in principle, be larger. However, comparison of Seto–van Duzer's $I_c(T)$ with the KL result for the same $\xi_{Sm}(T_c)$ reveals very different behavior already close to T_c. For completeness we note that, even within the GL context, Eq. (17) does not contain the full temperature dependence. The critical current has been obtained from

$$j_c=C[\Delta^+(d\Delta/dx)+\Delta(d\Delta^+/dx)]\ .$$

The factor $1/T$ in proportionality constant C has been omitted from the temperature dependence, probably based on the argument that the GL derivation is valid only for $T\approx T_c$, hence, $1/T$ is constant. However, already slightly below T_c this prefactor makes a significant difference. Fits to data have usually been extended to lower temperatures, where the difference is even more pronounced.

In summary, fits of SSmS data to the Seto–van Duzer theory published to date are based on unreliable expressions for the coherence length (except for n-type III-V compounds) and for the temperature dependence of $I_c(T)$. Although it was invariably concluded that agreement between theoretical $I_c(T)$ and ξ_{Sm} and experiment was good, it is clear that our observations invalidate this conclusion.

A well-known alternative for describing the temperature dependence of the critical current has been obtained by Likharev.[56] He has obtained $I_c(T)$ for arbitrary values of the temperature and junction length. For temperatures close to T_c he found

$$I_c(T)=\frac{2\Delta(T)^2}{\pi ekTR_N}\sum_n\frac{l_n(T)}{(2n+1)^2\sinh[l_n(T)]} \tag{21}$$

for junctions with normal state resistance R_N, with

$$l_n(T)=(2n+1)^{1/2}\frac{L}{\xi(T)}\ . \tag{22}$$

For long junctions this reduces to

$$I_c(T)=\frac{4\Delta(T)^2}{\pi kTR_N}\frac{L}{\xi_{Sm}(T)}\exp[-L/\xi_{Sm}(T)]\ . \tag{23}$$

Comparison with Eq. (18) shows that in Likharev's result the prefactor $1/T$ is present. Also, the absolute value of I_c is given, and not just the global temperature dependence. However, the theory has an important drawback, related to the treatment of the superconductor–normal-metal boundary. Likharev's results are based on boundary conditions first obtained by Zaitsev[58] which imply that the order parameter is continuous at the interface. Although the explicit use of these boundary conditions leads to quantitative predictions for I_c (as opposed to Seto–van Duzer), it severely restricts the applicability for semiconductor coupled weak links. The reason for this is that the effect of interface barriers on the supercurrent is not taken into account. It has been proposed to include this through a phenomenological scaling parameter for $I_c(T)$.[55,59] This approach is not compatible with Kupriyanov-Lukichev theory.[60] Although both theories are based on the same

microscopic Usadel equations for superconductivity in the dirty limit, they treat different systems. KL treat a SINIS system, with boundary conditions accounting for the interface barriers, whereas Likharev describes a SNS structure. The fundamental difference between the theories is illustrated by the fact that, for a given L/ξ_{Sm} and large boundary resistance, very different dependencies of the critical current on T are found. Although the underlying reasons are not clear, Likharev's $I_c(T)$ curves cannot be obtained from KL's curves by simply using a scaling factor.

In Fig. 18, we show that the application of theories with a restricted range of validity can yield very different values for the parameters, although good fits to the data are obtained. The measurements of Fig. 17 are replotted in Fig. 18, together with fits to Likharev's "near T_c" Eq. (21). The fits are scaled down to yield the measured I_cR_N products. Although the quality of the fits is good near T_c, they are insensitive to $L/\xi(T_c)$: data could be fitted equally well with values between 1.3 and 2.5 (sample $S1$), respectively, between 0.8 and 1.6. We have also fitted the data to the full Likharev theory. These fits are obtained from interpolation between curves shown in Ref. 56, again using a scaling factor. The good quality of the fit is probably fortuitous [fits to $I_c(T)$ of the other sample of Fig. 17 are of lesser quality]. The difference with the "near-T_c" fits is striking: $L/\xi(T_c)=5.5\pm0.3$ is found. Moreover the results of both the "near-T_c" and the full theory differ substantially from the KL result $L/\xi=2.3-2.4$ for both samples.

These findings show that, contrary to what one might naively expect, a scaled version of Likharev's theory should not be used for SSmS junctions. The barriers present at the metal-semiconductor interface require a separate treatment. We believe that this is appropriately done by KL, hence it presents the only useful description of SSmS systems.

B. Weak-localization effects

Up to this point, only supercurrent flow through the proximity effect has been discussed. Although KL theory describes the measurements well, it is interesting to analyze the possibility of an additional contribution to I_c through a different mechanism. This was introduced by Altshuler, Khmel'nitskii, and Spivak.[53] The authors consider, in the spirit of the quantum-interference phenomenon of weak localization, a phase-coherent path from one superconductor to the other. The path through the mesoscopic intermediate layer is determined by elastic scattering (Fig. 19). Andreev reflection has an important influence on carrier transport. If an electron is converted into a hole by Andreev reflection at the interface with the superconductor S_2, its phase changes with an amount equal to ϕ_2, the phase of the superconducting ground-state wave function. Subsequently, at the interface with S_1, the phase changes with $-\phi_1$, where the minus sign is added because the hole is converted back into an electron. To calculate the total effect of this process the time-reversed path must be included leading to a net phase difference of $2(\phi_1-\phi_2)$. As a consequence, a supercurrent I_c^A proportional to $\sin 2\phi$ ($\phi=\phi_1-\phi_2$) is predicted to flow parallel to the "ordinary" proximity-effect-induced supercurrent with the usual $\sin\phi$ dependence.

In principle, I_c^A could be observable at low temperatures. The authors state that an Andreev reflection probability $A(E)>l/\xi$ is required, which is much larger than the values we observe. However, in a later discussion[61] it is suggested that much smaller values for $A(E)$ suffice. The magnitude of I_c^A is given by

$$I_c^A(T)=\frac{2eDw^2}{\pi^2\xi_{Sm}^4(T)\ln(T_c/T)}\exp[-2L/\xi(T)] \qquad (24)$$

with w the width of the junction. The exponent dominating the temperature dependence is a factor of 2 larger than the exponent found in the above theories, for long junctions and T very close to T_c. Consequently, the decrease of this contribution with temperature is much more rapid. Assuming $A(E)$ to be large enough in the present experimental system, we calculate values for I_c^A of a few μA at 1.2 K, for $L/\xi(T_c)=2.3$. This constitutes only a few percent of the measured values. Hence, a possible contribution of I_c^A will be difficult to infer from the measured temperature dependence of the critical current.

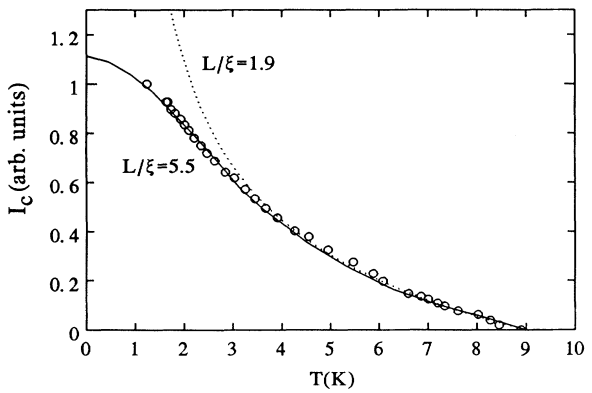

FIG. 18. Critical current vs temperature for one of the samples from Fig. 17, together with fits to Likharev's theory. Solid curve: full theory, dotted curve: near-T_c approximation.

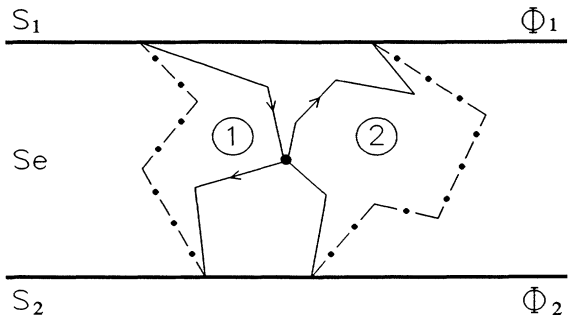

FIG. 19. Example of phase-coherent scattering paths in a heavily doped semiconductor (Sm) sandwiched between two superconductors S_1 and S_2 with phase ϕ_1 and ϕ_2, respectively. Drawn lines indicate electrons that are Andreev reflected into holes (dot-dashed lines) at the interfaces.

A more clear-cut identification should be possible through the phase dependence. To identify a possible $\sin 2\phi$ dependence we have investigated both the magnetic-field dependence of I_c and its response to rf radiation. The ac Josephson effect gives rise to the presence of current steps in the I,V characteristic when rf radiation is applied to the junction. The distance between the steps V_0 is determined by the irradiated frequency ω according to $V_0=\hbar\omega/2e$. It is easy to show that if the phase dependence of I_c is $\sin 2\phi$ instead of $\sin\phi$ the distance will be $V_0=\hbar\omega/4e$. We have irradiated the samples discussed in Sec. IV A 2 and others with 10-GHz radiation and have observed clear steps at 20 μV. These steps correspond to $\hbar\omega/2e$ and confirm the presence of the usual ac Josephson effect. We do not find any trace of 10-μV steps that would confirm the presence of the weak-localization-mediated contribution.

The response of the critical current of sample $S1$ to a magnetic field B, applied parallel to the junction, is shown in Fig. 20. The well-known Fraunhofer diffraction pattern for Josephson junctions is observed. Theoretically, I_c is periodic in the magnetic flux Φ through the junction, with period Φ_0 equal to the flux quantum $h/2e$:[62]

$$I_c(B)=I_c(0)\frac{\sin(\pi\Phi/\Phi_0)}{\pi\Phi/\Phi_0}=I_c(0)\frac{\sin(\pi B/B_0)}{\pi B/B_0} \quad (25)$$

with $B_0=\Phi_0/S$ and S the junction area defined below. At magnetic field B_0 the junction contains one fluxquantum. The theoretical curve in Fig. 20 has been obtained by setting B_0 in Eq. (25) equal to 2.17×10^{-4} T. The good agreement of the data with the diffraction pattern implies a uniform distribution of the current in the junction.[63] We note in passing that this observation is in favor of the earlier discussed picture of a large number of small transparent "spots" distributed over the interface (as opposed to one larger transparent "spot"). A $\sin 2\phi$ dependence of I_c, instead of the $\sin\phi$ dependence leading to Eq. (25), will result in a similar diffraction pattern as the one shown in Fig. 20, with the important modification that the period will equal $\Phi_0/2$ instead of

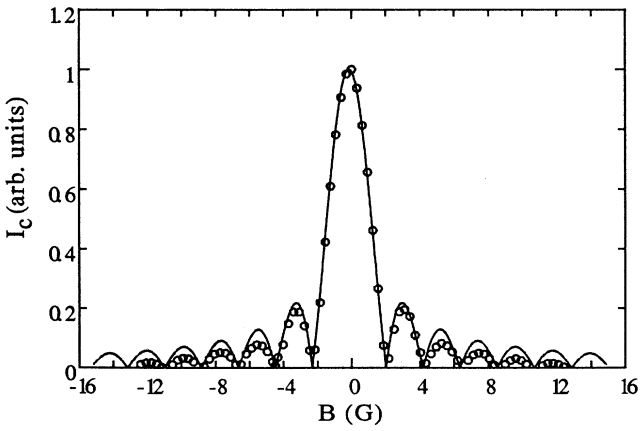

FIG. 20. Critical current as a function of the applied magnetic field B (dots). The solid curve represents the theoretical Fraunhofer pattern for an ideal junction, with period 2.17 G.

Φ_0. Comparison of the value used for B_0 in Fig. 20 to the theoretical magnetic field corresponding to the full period of the regular Josephson effect, $B_0=\Phi_0/S=2.07\times10^{-15}$ Tm^2/S, can decide whether the weak localization effect is present. The area S in Eq. (25) corresponds to the current-carrying area effectively threaded by the magnetic flux parallel to the junction surface. It is defined as the product of the junction effective thickness $d_{\rm eff}$ and the width of the junction. The thickness $d_{\rm eff}$ is defined in terms of the membrane thickness L, superconductor thickness d, and the London penetration depth λ by $d_{\rm eff}=L+2\lambda\tanh(d/2\lambda)$. This expression takes into account the penetration of the magnetic field into the superconducting electrodes over a depth λ. The theoretical expression for the penetration depth at low temperature is $\lambda=\lambda_0(1+\xi_0/l)$, with l the elastic mean free path in the superconductor and ξ_0 the BCS coherence length.[64] The mean free path is obtained from the ρl product for niobium,[65] 3.7×10^{-6} Ω cm^2, and the resistivity measured for 300-nm niobium films, $\rho=5.5\mu\Omega$ cm. Substituting $l=6.7$ nm and $\xi_0=38$ nm (Ref. 66) yields $\lambda=103$ nm. This value is slightly larger than the values 84–91 nm inferred from the literature, for niobium films comparable to ours.[67] A smaller λ (81 nm) is also obtained from

$$\lambda^2=\frac{\hbar\rho}{\pi\mu_0\Delta(T=0)} \quad (26)$$

with μ_0 the vacuum magnetic permeability. We conclude that the best estimate for the niobium electrodes is $\lambda=90\pm10$ nm. This yields $d_{\rm eff}=0.21$ μm, the area $S=2.3$ μm^2, and the desired theoretical value for $B_0=9.0\times10^{-4}$ T. The experimental value of 2.17×10^{-4} T for sample $S1$, inferred from Fig. 20, is a factor of 4 smaller. For different samples, we find the measured period a factor of about 2–4 smaller than the period calculated from Eq. (25). Although it is tempting to ascribe the factor 2 to the effect we are looking for, the deviation varies randomly between 2 and 4 and may be due to other effects.

The most probable of these is that the magnetic field present in the junction region differs from the applied magnetic field.[68] The samples consist of two niobium electrodes of 2000×3000 μm^2 separated by 250-μm silicon. In the pyramidal etchpit, the sidewalls are covered with niobium, and towards the bottom of the pit the electrodes approach each other. Only in the junction region they are very close together, separated by just the thin membrane (Figs. 1 and 2). Possibly, the Meissner effect in the electrodes leads to crowding of magnetic flux lines and an increase of B in this region explaining the relatively small values measured for B_0. We note that this effect has previously been observed in Nb-InAs-Nb junctions.[69] In this work the effect is quite strong due to the coplanar geometry of these junctions.

In conclusion, the rf and magnetic-field dependences of I_c demonstrate the dc and ac Josephson effect in the junctions. Although no evidence for the weak localization mechanism proposed by Altshuler, Khmel'nitskii, and Spivak[53] is found, its presence cannot be entirely excluded on the basis of our experimental data. The strength of

the effect compared to the "ordinary" proximity effect supercurrent is not well known and it is probably weak in our junctions. In cleaner systems with more transparent interfaces, the mechanism may be more clearly present.

V. SUMMARY AND CONCLUSIONS

In this work we have presented experimental results on transport at finite voltages and supercurrent flow in a well-characterized, sandwich-type superconductor-semiconductor-superconductor system. The combined investigation of I_c and the behavior at $V \neq 0$ considerably increases the insight in these systems. We have demonstrated that the I,V characteristics at low temperatures can be well understood in terms of the OBTK model described in Sec. III A. The model describes a SINIS structure: a SNS system with variable elastic and Andreev scattering at the interface barriers I. Inelastic scattering is assumed to be absent in N. The validity of this assumption is confirmed by the observation of higher-order Andreev reflections at low voltages, and a current deficit at high V. For an optimal description, the possibility of two interface barriers of different strengths (expressed by the dimensionless parameter Z) has to be included. Additionally, there may be small differences in the silicon valence band at the two interfaces due to variations of the doping profile with the thickness of the Si membrane.

Given the good quality of the fits to the OBTK model at low temperatures, an unambiguous description of the behavior at higher temperatures should be possible. As we have shown, self-heating plays an important role above the λ-point, making a direct application of the model at higher temperatures difficult. Additionally, temperature-dependent inelastic scattering may be present, further complicating the analysis at elevated temperatures.

An interesting result of the application of the OBTK model to our system is that only a small fraction of the superconductor-semiconductor interfaces is transparent. Moreover, this area is likely to be distributed more or less uniformly over the interfaces as small transparent "spots." The overall transparency of such an interface poses a challenging theoretical problem that is currently of interest to the field of Schottky barriers. The Z values that we measure indicate a transparency that is much too high to be explained by standard Schottky barrier theory.

We note that a lower limit to the interface transparency is present in any superconductor-semiconductor structure: the mismatch in the Fermi wave vector between metal and semiconductor results in the presence of an intrinsic barrier at their interface. The reflection and transmission properties of the interface barrier determine the detailed shape of the I,V characteristics but also govern the reduction of the critical current through the structure. Consequently, an adequate treatment of supercurrent flow must account for the presence of interface barriers.

The absence of inelastic scattering in silicon implies that the system is mesoscopic. In principle, two parallel channels for supercurrent transport are possible. One is the conventional proximity effect: the pair correlation between electrons present in the superconductors diffuses over a characteristic length into the intermediate material. The most advanced treatment of the proximity effect in a SINIS structure is the theory of Kupriyanov and Lukichev,[15] which is discussed in Sec. IV A 1. It is by far the most complete description of supercurrent transport through a normal metal with $l < L$. Besides describing the whole temperature range it takes into account the discontinuity in the superconducting order parameter at the SmS interface. Excellent agreement between the supercurrent measurements and Kupriyanov-Lukichev theory is obtained for the whole temperature range. The discrepancy between the value for the coherence length inferred from the KL analysis and the theoretical value indicates the need for a careful analysis of the effect of the band structure of p-Si on transport properties. Additionally, we have shown that several earlier models used to interpret supercurrent measurements are unsuitable for semiconductor coupled weak links.

The other channel for supercurrent transport is based on the combination of Andreev reflections at the interfaces with weak localization effects in the intermediate mesoscopic layer.[53] For completeness we have also investigated this channel, focusing on the $\sin 2\phi$ phase dependence that is predicted for it. Both the magnetic field and rf dependences of the critical current do not show any direct evidence for the presence of this mechanism.

ACKNOWLEDGMENTS

The authors thank S. L. Wang for skillful electron microscopy as well as L. de Lange for assistance during the initial experiments. We acknowledge fruitful discussions and correspondence with M. Yu. Kupriyanov, A W. Kleinsasser, and A. F. Volkov. This work was supported by the Netherlands Organization for Scientific Research (NWO) through the Foundation for Fundamental Research on Matter (FOM).

APPENDIX

We discuss the values for the carrier concentration, mobility, and effective mass that are used to calculate the semiconductor coherence length ξ_{Sm} in our samples. As explained in Sec. III E, the carrier concentration $n = 7 \times 10^{19}$ cm^{-3} is the average value derived from the theoretical doping profile (Fig. 14). The carrier concentration is assumed to equal the boron concentration. This estimate is subject to some uncertainty, but the dependence of ξ_{Sm} on carrier concentration is weak. If n were a factor of 1.5 higher than estimated, the increase of ξ_{Sm} would be only about 14%. We note that the carrier concentration dependence of μ[70] and m^* tends to offset this increase.

We estimate the mobility $\mu = 116$ cm^2/V s from the relation $\mu = 1/ne\rho$, with $\rho = 7.7 \times 10^{-4}$ Ω cm the measured resistivity of the silicon membrane. In addition to the uncertainty in n, the uncertainty in ρ introduces 10–15 % uncertainty in the value for μ. In other weak-link experiments on p-Si,[71] μ or ρ has not been measured but

"reasonable" values of 60–100 cm^2/s have been used for the mobility.

The effective mass of silicon has been studied by several authors, and some controversy exists on the exact values for m^*.[72] We follow the article by Barber.[57] On the basis of a simplified model for the valence band of Si, he obtains reasonable agreement with experimental data on the temperature and carrier concentration dependence of m^*. Using his data, we find the conductivity effective mass $m_c^*=0.43$ and the density-of-states mass $m_d^*=0.87$ for $n=7\times10^{19}$ cm^{-3}. For high doping the sensitivity of the effective mass to n is very weak.

Substantially larger values for ξ_{Sm} in our samples can only be obtained from Eq. (13) with a much smaller ratio m_d^{*2}/m_c^*. This quantity has the dimensions of mass and equals 1.76. We calculate the m^* values that have been used in Ref. 71 to obtain ξ_{Sm} from Seto and Van Duzer's equation [Eq. (19)] to be 0.39, 0.24, and 0.50, respectively. The origin of these values has not been discussed by the authors.

[1]P. G. DeGennes, Rev. Mod. Phys. **36**, 225 (1964).

[2]J. Clarke, Proc. R. Soc. London, Ser. A **308**, 447 (1969).

[3]J. Seto and T. van Duzer, in *Low Temperature Physics LT13,* edited by K. D. Timmerhaus, W. J. O'Sullivan, and E. F. Hammel (Plenum, New York, 1974), p. 328.

[4]I. O. Kulik, Zh. Eksp. Teor. Fiz. **57**, 1745 (1969) [Sov. Phys. JETP **30**, 944 (1970)].

[5]J. Bardeen and J. L. Johnson, Phys. Rev. B **1**, 72 (1972).

[6]B. J. van Wees, K.-M. H. Lenssen, and C. J. P. M. Harmans, Phys. Rev. B **44**, 470 (1991).

[7]A. Furusaki and M. Tsukada, Phys. Rev. B **43**, 10 164 (1991).

[8]C. W. J. Beenakker and H. van Houten, Phys. Rev. Lett. **66**, 3065 (1991).

[9]R. Kümmel, U. Schüssler, U. Gunsenheimer, and H. Plehn, Physica C **185-189**, 221 (1991).

[10]A. Furusaki, H. Takayanagi, and M. Tsukada, Phys. Rev. Lett. **67**, 132 (1991).

[11]For a review, see A. W. Kleinsasser and W. J. Gallagher, in *Modern Superconducting Devices,* edited by D. Rudman and S. Ruggiero (Academic, Boston, 1989); T. M. Klapwijk, D. R. Heslinga, and W. M. van Huffelen, in *Superconducting Electronics,* edited by H. Weinstock and M. Nisenoff (Springer, Berlin, 1989).

[12]T. Nishino, M. Miyake, Y. Harada, and U. Kawabe, IEEE Electron Dev. Lett. **EDL4-6**, 297 (1985).

[13]H. Takayanagi and T. Kawakami, Phys. Rev. Lett. **54**, 2449 (1985).

[14]Z. Ivanov, T. Claeson, and T. Anderson, Jpn. J. Appl. Phys. **26**, 1617 (1987).

[15]M. Yu. Kuprianov and V. F. Lukichev, Zh. Eksp. Teor. Fiz. **94**, 139 (1988) [Sov. Phys. JETP **67**, 1163 (1988)].

[16]W. M. van Huffelen, M. J. de Boer, and T. M. Klapwijk, Appl. Phys. Lett. **58**, 2438 (1991).

[17]D. R. Heslinga, W. M. van Huffelen, and T. M. Klapwijk, IEEE Trans. Magn. **27**, 3264 (1991).

[18]A. W. Kleinsasser, T. N. Jackson, D. McInturff, F. Rammo, G. D. Pettit, and J. M. Woodall, Appl. Phys. Lett. **57**, 1811 (1990).

[19]G. A. Ovsyannikov and G. E. Babayn, Physica B **168**, 239 (1991).

[20]D. R. Heslinga and T. M. Klapwijk, Solid State Commun. **84**, 739 (1992).

[21]T. M. Klapwijk, G. E. Blonder, and M. Tinkham, Physica B **109&110**, 1657 (1982).

[22]M. Octavio, M. Tinkham, G. E. Blonder, and T. M. Klapwijk, Phys. Rev. B **27**, 6739 (1983).

[23]T. M. Klapwijk, in *SQUID'85—Superconducting Quantum Interference Devices and their Applications,* edited by H. D. Hahlbohm and H. Lübbig (De Gruyter & Co., Berlin, 1985).

[24]A. F. Andreev, Zh. Eksp. Teor. Fiz. **46**, 1823 (1964) [Sov. Phys. JETP **19**, 1228 (1964)].

[25]G. E. Blonder, M. Tinkham, and T. M. Klapwijk, Phys. Rev. B **25**, 4515 (1982).

[26]W. M. van Huffelen, T. M. Klapwijk, and L. de Lange, Phys. Rev. B **45**, 535 (1992).

[27]K. Flensberg, J. Bindslev Hansen, and M. Octavio, Phys. Rev. B **38**, 8707 (1988).

[28]E. L. Wolf, *Principles of Electron Tunneling Spectroscopy* (Oxford University Press, New York, 1985).

[29]K. K. Likharev, Rev. Mod. Phys. **51**, 101 (1979).

[30]M. Yu. Kupriyanov and V. F. Lukichev, Fiz. Nizk. Temp. **8**, 1045 (1982) [Sov. J. Low Temp. Phys. **8**, 526 (1983)].

[31]A. A. Zubkov and M. Yu. Kupriyanov, Fiz. Nizk. Temp. **9**, 548 (1983) [Sov. J. Low Temp. Phys. **9**, 279 (1983)].

[32]W. M. van Huffelen, T. M. Klapwijk, and E. P. Th. M. Suurmeijer, Phys. Rev. B **47**, 5151 (1993).

[33]D. R. Heslinga and T. M. Klapwijk, Appl. Phys. Lett. **54**, 1049 (1989).

[34]S. M. Sze, *Physics of Semiconductor Devices,* 2nd ed. (Wiley, New York, 1981).

[35]A. Fernandez, H. D. Hallen, T. Huang, R. A. Buhrman, and J. Silcox, Appl. Phys. Lett. **57**, 2826 (1990).

[36]J. Y. Cheng and L. J. Cheng, Appl. Phys. Lett. **58**, 45 (1991); S. R. Mahamuni, D. T. Abell, and D. Williams, Solid State Commun. **68**, 145 (1988).

[37]G. E. Blonder and M. Tinkham, Phys. Rev. B **27**, 112 (1983).

[38]W. J. Skocpol, M. R. Beasley, and M. Tinkham, J. Appl. Phys. **45**, 4044 (1974).

[39]M. G. Hauser and D. W. Palmer, Rev. Phys. Appl. **9**, 53 (1974).

[40]G. L. Pollack, Rev. Mod. Phys. **41**, 48 (1969).

[41]S. Kaplan, J. Low Temp. Phys. **37**, 343 (1979).

[42]S. K. Decker and D. W. Palmer, J. Appl. Phys. **48**, 2043 (1977).

[43]In Ref. 38, α(Sn-sapphire or glass)=1–3.5 W/cm^2K is found at about 3 K. In Ref. 42, α(Ta-Si)=0.5–2.0 W/cm^2K and α(Ta-sapphire)=1–4 W/cm^2K, at $T=3$–4 K. Applying Kaplan's theory (Ref. 41) we find the following theoretical values for the corresponding temperatures: α(Ta-Si)=0.5–1.1 W/cm^2K and α(Sn-sapphire)=0.5. The reasonable agreement with the experimental values gives us some confidence in the calculated value for α(Nb-Si).

[44]K. Mittag, Cryogenics **2**, 94 (1973).

[45]We note that the absence of heating at 1.2 K, assumed at the beginning of this section, is supported by the quality of the fits at 1.2 K to the OBTK model. The upward bend of the

measured I,V curve above $eV \approx \Delta$, and the kink due to the superconducting-normal transition of the electrodes, which are indications of heating (Fig. 11), are absent at 1.2 K. Moreover, the power dissipated at $V = V_2$, corresponding to the $n = 2$ dip, is about an order of magnitude smaller than the power dissipated at $V = V_1$, corresponding to the $n = 1$ dip. Consequently, in the presence of heating, the $n = 1$ dip should be much more shifted towards lower voltages than the $n = 2$ dip, and agreement of the dip positions with the model calculations would not occur. A heating-induced depression of the $n = 1$ dip from 3.05 to the measured value of 2.62 mV (Fig. 3) implies a temperature rise of about 5 K. At $V = V_2$ the temperature rise would be about 0.5 K, implying a negligible shift in the position of the $n = 2$ dip, which should thus occur at about $3.05/2 = 1.52$ mV. This is clearly not the case. Consequently, the fact that the subharmonic gap structure is found at the predicted positions, for $n = 1, 2, \ldots$, supports the assumed absence of heating at 1.2 K. See also W. J. Skocpol and M. Tinkham, IEEE Trans. Mag. **13**, 739 (1977); Phys. Rev. B **17**, 159 (1978).

[46]J. Nitta, H. Nakano, T. Akazaki, and H. Takanayagi, in *Single-Electron Tunneling and Mesoscopic Devices,* edited by H. Koch and H. Lübbig (Springer, Berlin, 1992), p. 295.

[47]R. Kümmel, U. Gunsenheimer, and R. Nicolsky, Phys. Rev. B **42**, 3992 (1990).

[48]D. E. Cullen, E. L. Wolf, and D. Compton, Phys. Rev. B **2**, 3157 (1970).

[49]R. G. Wilson, J. Appl. Phys. **54**, 6883 (1983); Y. H. Li, A. P. Pogany, H. B. Harrison, and J. S. Williams, Nucl. Instrum. Methods B **19/20**, 521 (1987).

[50]L. P. Gorkov, Zh. Eksp. Teor. Fiz. **36**, 1918 (1958) [Sov. Phys. JETP **9**, 1364 (1959)].

[51]K. D. Usadel, Phys. Rev. Lett. **25**, 507 (1970).

[52]P. G. de Gennes, *Superconductivity of Metals and Alloys* (Benjamin, New York, 1966).

[53]B. L. Altshuler, D. E. Khmel'nitskii, and B. Z. Spivak, Solid State Commun. **48**, 8 (1983).

[54]A review of the analysis of weak links based on high-T_c superconductors, within the framework of KL theory is M. Yu. Kupriyanov and K. K. Likharev, Usp. Fiz. Nauk **160-162**, 49 (1990) [Sov. Phys. Usp. **33**, 340 (1990)].

[55]D. R. Heslinga, Ph.D. thesis, University of Groningen, 1991 (unpublished).

[56]K. K. Likharev, Pisma Zh. Tekh. Fiz. **2**, 29 (1976) [Sov. Phys. Tech. Lett. **2**, 12 (1976)].

[57]H. D. Barber, Solid State Electron. **10**, 1039 (1967).

[58]R. O. Zaitsev, Zh. Eksp. Teor. Fiz. **50**, 1055 (1966) [Sov. Phys. JETP **23**, 702 (1966)].

[59]R. B. van Dover, A. de Lozanne, and M. Beasley, J. Appl. Phys. **52**, 7327 (1981); A. W. Kleinsasser, IEEE Trans. Magn. **MAG-27**, 2589 (1991).

[60]M. Yu. Kupriyanov, private communication.

[61]B. L. Altshuler and A. G. Aronov, in *Electron-Electron Interactions in Disordered Systems,* edited by A. L. Efros and M. Pollak (North-Holland, Amsterdam, 1985).

[62]A. Barone and G. Paterno, *Physics and Applications of the Josephson Effect* (Wiley, New York, 1982).

[63]Additionally, distortion of the diffraction pattern due to the magnetic field of the supercurrent itself is negligible. The absence of self-field effects is also implied by a comparison of the junction width (10.9 μm) with the parameter λ_J, the so-called Josephson penetration depth (Ref. 62), for which 33 μm is found.

[64]M. Tinkham, *Introduction to Superconductivity* (McGraw-Hill, New York, 1975).

[65]A. F. Mayadas, R. B. Laibowitz, and J. J. Cuomo, J. Appl. Phys. **43**, 1287 (1972); C. M Soukoulis and D. A. Papaconstantopoulos, Phys. Rev. B **26**, 3673 (1982).

[66]T. van Duzer and C. W. Turner, *Principles of Superconducting Devices and Circuits* (Elsevier North-Holland, New York, 1981).

[67]J. H. Greiner *et al.*, IBM J. Res. Dev. **24**, 195 (1980); R. F. Broom, J. Appl. Phys. **47**, 5432 (1976); K. Schwidtal, *ibid.* **43**, 202 (1972).

[68]Two other possibilities can be ruled out. First, the niobium resistivity quoted has been measured on a separate film, prepared simultaneously with the junctions. In principle, the niobium films covering the membrane could have a higher resistivity, resulting in a penetration depth larger than the estimated value. This would lead to a larger d_{eff} and smaller theoretical value for B_0. However, the dependence of B_0 on ρ is much too weak to allow a decrease of B_0 by a factor of 4. Second, a supercurrent flowing predominantly through the middle of the junction would lead to a reduction of the period B_0 (Ref. 62). However, this would also result in an $I_c(B)$ dependence different from the $\sin(x)/x$ that we measure.

[69]K. Inoue and T. Kawakami, J. Appl. Phys. **65**, 1631 (1989). We calculate a ratio of actual magnetic field to applied field of 10–50 for the samples reported.

[70]G. Masetti, M. Severi, and S. Solmi, IEEE **ED-27**, 764 (1983).

[71]R. C. Ruby and T. van Duzer, IEEE Trans. Electron. Dev. **ED-28**, 1394 (1981); T. Nishino, E. Yamada, and U. Kawabe, Phys. Rev. B **33**, 2042 (1986); M. Hatano, T. Nishino, F. Murani, and U. Kawabe, Appl. Phys. Lett. **53**, 409 (1988).

[72]A recent review is M. A. Green, J. Appl. Phys. **67**, 2944 (1990).

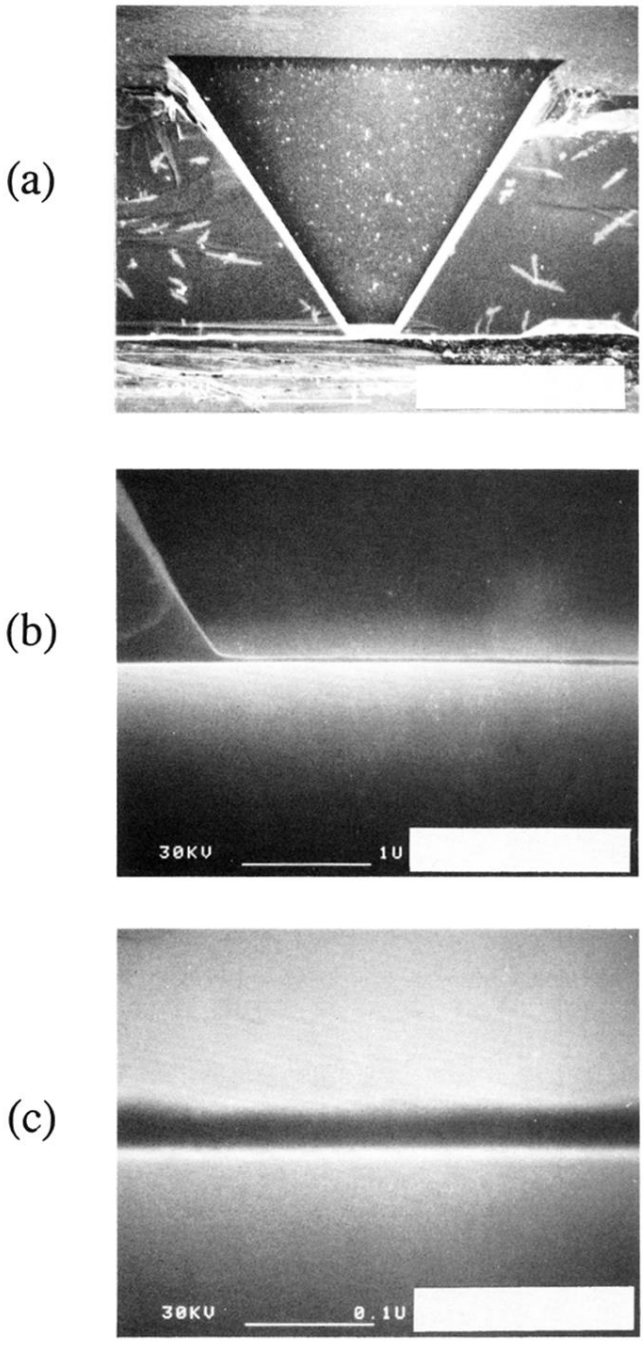

FIG. 2. Scanning electron microscope photographs of a silicon membrane cross section. (a) Full cross-section of the part of the chip containing the etchpit. The width of the pyramidal pit at the top surface is about 400 μm, the width of the membrane at the bottom of the pit equals 40 μm. (b) Corner of the bottom of the pit plus membrane. (c) Detail of the membrane.

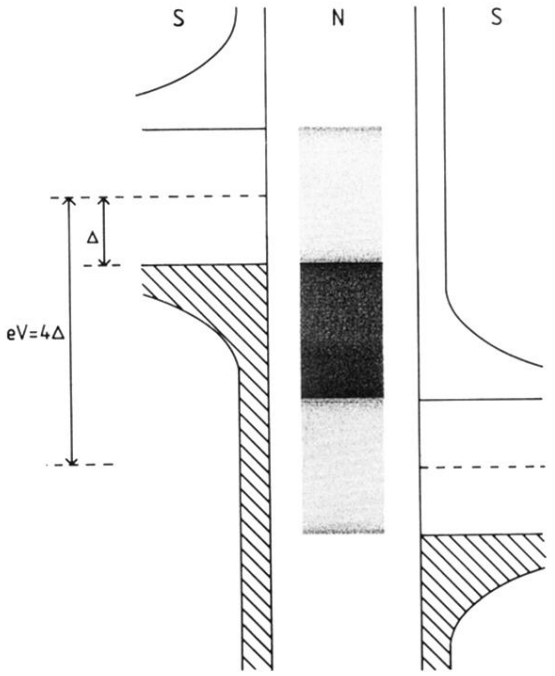

FIG. 5. Current transport through the normal region in a SINIS structure with $Z=2.0$ at $eV=4\Delta$ and $T=0$. The energy scale is plotted vertically, while the density of states in the left and right superconducting electrodes is plotted horizontally. Filled states in the electrodes are shaded. The current density in N is represented by the blackness (open: zero current, solid: high current). The high Andreev reflection coefficient at the gap edges leads to large current contributions of energy levels in N opposite the edges, just inside the gap.